PERGAMON

Journal of Structural Geology 22 (2000) 1675–1693

JOURNAL OF STRUCTURAL GEOLOGY

www.elsevier.nl/locate/jstrugeo

Grain boundary contact effects during faulting of quartzite: an SEM/EBSD analysis

Geoffrey E. Lloyd*

School of Earth Sciences, The University, Leeds LS2 9JT, UK

Received 12 November 1999; accepted 25 May 2000

Abstract

During low-temperature faulting of Cambrian quartzite (Assynt, NW Scotland), stress concentrations develop at grain contacts either at the onset of deformation, prior to the establishment of a through-going fault plane, or within the damage zone remote from the main displacement segment. Such concentrations contribute to the development of intragranular microfractures, cataclastic microstructures and fault rocks. This contribution considers the progressive deformation sequence that precedes microfracturing and cataclasis. The complexity of this deformation is revealed by scanning electron microscope (SEM) electron backscattered diffraction (EBSD). Dauphiné twinning is a widespread feature associated with grain contact stress concentration and forms distinctive EBSD microstructures. Automatic SEM/EBSD analysis reveals that whilst initial indentation causes dauphiné twinning of many grains, continued indentation results in the formation of an arcuate array of subgrains via low temperature plasticity and/or microcracking, which overprint the dauphiné twins. These observations are consistent with transmission electron microscopic analysis of quartz crystals used for microhardness indentation tests, which reveal that indentation causes an intensely deformed region to develop, comprising a high density of microfractures and a submicron scale 'blocky' microstructure that accommodates any 'plastic' deformation. Deformation mechanisms and associated microstructures develop sequentially with progressive indentation and may provide sites of microfracture nucleation via low-temperature ductile fracture. The new microstructures assist diffusive mass transfer (DMT) processes by the formation of a cellular or subgrain array that represents a reduction of several orders of magnitude in apparent grain size and hence in diffusion path length. Concomitantly, associated microfracturing perturbs local thermodynamic equilibrium, leading to enhanced DMT, crack healing and cementation overgrowths. Together, these processes form the aseismic creep and sealing components of fault zone development. Published by Elsevier Science Ltd.

1. Introduction

Over recent years the study of faults and faulting has received considerable attention. A combination of field, microstructural, experimental and theoretical analyses has led to significant advancement in our understanding of faulting processes. These investigations have been stimulated by the realisation that faulting plays a significant role in earthquake rupture processes and the geological evolution of hydrocarbon reservoirs and formation of ore deposits, particularly incorporating fluid migration and entrapment. (For extensive reviews, see: Kranz, 1983; Kirby, 1984; Rutter et al., 1986; Sibson, 1986; Tullis, 1986; Wang, 1986; Atkinson, 1987; Mitra, 1988; Marone and Scholz, 1989; Scholtz, 1989; Knipe and Rutter, 1990; Larsen et al., 1992; Marone and Blanpied, 1994; Jones et al., 1998; Snoke et al., 1998.)

As a result of these studies, we now know that the faulting process is not confined to a discrete failure surface or displacement plane. Rather, it involves a 'zone' of distributed deformation (e.g. Fig. 1a) extending for some distance into both the hanging and foot walls (e.g. Knipe, 1992a,b; McGrath and Davison, 1995; Vermilye and Scholz, 1998; Vermilye and Scholz, 1999). Faults nucleate by the progressive concentration of deformation (Adams and Sines, 1978; Hippler and Knipe, 1990; Anders and Wiltschko, 1994; Moore and Lockner, 1995). They then propagate spasmodically (seismically) into a 'process' zone that develops slowly (aseismically) ahead of the active fault tip. As the fault tip propagates through its process zone, it leaves behind a 'wake' zone of damage on either side of the fault plane. This zone may continue to develop microstructurally long after the fault tip has propagated through, in the *reduced* stress and/or strain fields associated with faulting. Thus, although fracturing dominates during faulting, leading to the classic cataclastic fault rock microstructure (e.g. Fig. 1b), a range of other low temperature deformation mechanisms must also occur (e.g. Groshong,

* Corresponding author.
E-mail address: g.lloyd@earth.leeds.ac.uk (G.E. Lloyd).

0191-8141/00/$ - see front matter. Published by Elsevier Science Ltd.
PII: S0191-8141(00)00069-9

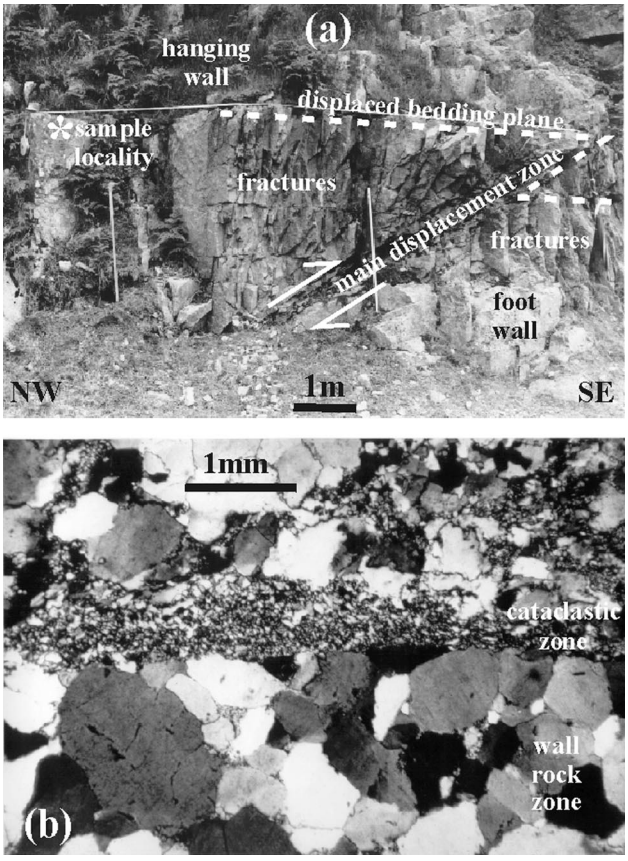

Fig. 1. (a) The Skiag Bridge back thrust fault zone, Assynt, NW Scotland. (b) Examples of cataclastic fault rock and wall rock microstructures (cross-polars).

1988; Knipe, 1989). Together, these disparate mechanisms contribute to the evolution of the 'damage' zone, as well as the main fault plane, and ultimately contribute to fault displacement. It is now known (e.g. Lloyd and Knipe, 1992; Knipe and Lloyd, 1994) that low-temperature plasticity (LTP), via dislocation glide, and diffusive mass transfer (DMT) processes make significant contributions to fault zone evolution and the formation of cataclastic fault rock microstructures.

LTP promotes strain hardening on both the local (grain) and fault zone scales, leading eventually to fracture (Groshong, 1988; Knipe, 1989). Fractures may be extensional mode I, shear mode II, or a combination of modes I and II (Mitra, 1984; Lloyd and Knipe, 1992). Fracture therefore is not necessarily a single mechanism but a range of mechanisms (often time dependent) and/or combination of complex processes. These include, cleavage fracture (types I, II and III), brittle intergranular fracture (types I, II and III) and low-temperature ductile fracture (LTDF), depending on the amount of pre-fracture plastic deformation (e.g. Ashby et al., 1979; Ghandi and Ashby, 1979; Atkinson, 1987; Ewalds and Wanhill, 1989; Lloyd and Knipe, 1992). DMT processes (e.g. Groshong, 1988; Knipe, 1989) aid compaction and cementation processes, which exercise important controls on fault zone strength evolution and fluid flow properties due to the tendency for faults to 'seal'. Fault sealing typifies the aseismic quiescent periods that characterise most of the fault zone evolution history. DMT involves solution at a source, transportation from this source and precipitation at a sink (Knipe, 1989). It is intimately related therefore to fracture but, as we shall see in this contribution, it may also be linked to LTP processes.

The periodic aseismic–seismic concept of fault zone evolution contrasts markedly with the traditional linear elastic fracture mechanics interpretations and has more in common with the critical opening displacement or J-integral models of non-linear fracture mechanics (Atkinson, 1987; Knott, 1979). In these approaches, damage zones develop via void nucleation and coalescence prior to a sudden critical and significant advance of the crack tip. Knipe and Lloyd (1994) have proposed that fault zone processes can be distinguished in terms of position and/or time. The former recognises that deformation rates change with position during fault zone evolution and is similar to the concept of process and wake zones. The latter recognises the change in differential stress and hence deformation mechanisms with time. However, in spite of improved and sophisticated models of fault zone evolution, there is still much to learn about the behaviour of faults and faulting. In particular, new techniques of microstructural analysis can now provide major insights into faulting processes. In this contribution, recently established scanning electron microscope (SEM) techniques are used to image fault zone microstructures that have hitherto remained unrecognised. This approach reveals a progressive deformation sequence on the grain scale, which represents a precursor to fault tip propagation within the process zone and/or a far field strain reaction within the wake zone.

2. Geological and analytical background

2.1. Specimen description

The samples considered in this study were collected from a minor back thrust fault developed in the Pipe Rock Member of the Cambrian Eriboll Quartzite Formation (Swett, 1969) at Skiag Bridge, Assynt, NW Scotland. Here, thrusting to the WNW of a Cambro-Ordovician sedimentary sequence, Precambrian Lewisian Gneisses and Moine Schists has produced a total displacement of >100 km (Christie, 1963; McClay and Coward, 1981; Coward, 1983, 1985; Elliott and Johnson, 1980; Butler, 1984; Butler and Coward, 1984). Deformation conditions in the Assynt region have been estimated at 200–250°C and 2–3 kb or 6–9 km (Johnson et al., 1985). There have been relatively few studies of the cataclastic fault rocks of the Moine Thrust Zone (e.g. Weathers et al., 1979; Blenkinsop and Rutter, 1986; Bowler, 1989; Hippler and Knipe, 1990; Knipe, 1990). The Skiag Bridge fault (Lloyd and Knipe, 1992;

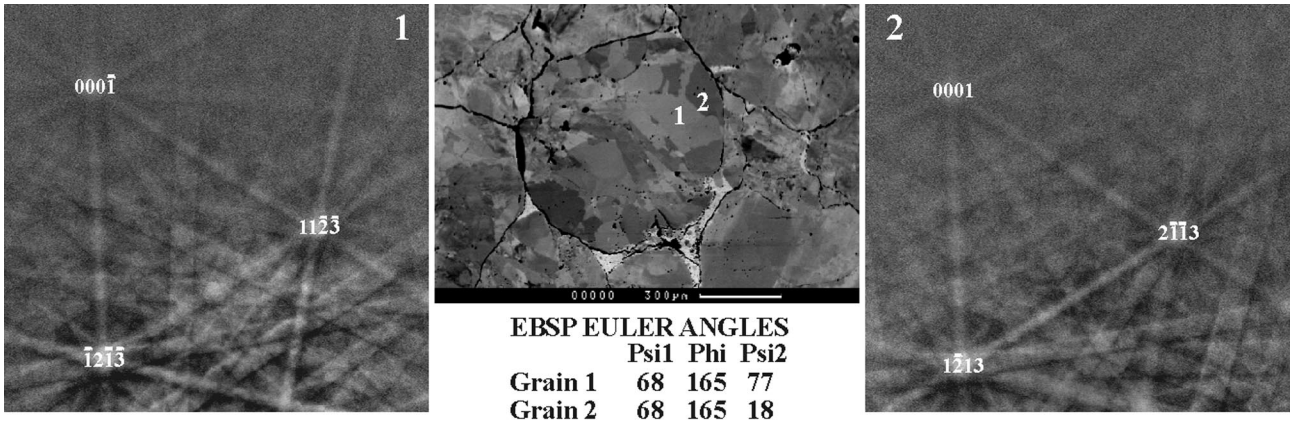

Fig. 2. Example of SEM/EBSD analysis and quartz pseudo-symmetry. *Centre*, FSE image of intragranular microstructure. *Left* and *right*, EBSPs obtained from regions 1 and 2 are similar but close examination reveals subtle differences explained by 59° rotation about the ***c***-axis (i.e. the third Euler angle, Psi2), consistent with dauphiné twinning.

Knipe and Lloyd, 1994) is a minor E–W trending back thrust (oblique ramp) that strikes ~40° to the regional movement direction (Fig. 1a). Although it apparently occurs in the immediate foreland to the traditional Sole Thrust to the Moine Thrust Zone (Peach et al., 1907), Coward (1984, 1985) recognised a structurally lower 'sole' with a displacement of ~3 km. The Skiag Bridge back thrust occurs in the immediate hanging wall to this feature and has accommodated ~1 m of displacement on a ~30 cm wide movement zone. However, an adjacent damage zone is observed in both hanging and foot walls (Fig. 1a).

This contribution concentrates on samples collected from the same bed of well-sorted and rounded grains, ranging in size up to a few millimetres, in the hanging wall remote to the movement plane (see Knipe and Lloyd, 1994, Fig. 3). Many grains have suffered DMT processes before, during and after faulting. Quartz precipitated via DMT processes during faulting exhibits poor or zero cathodoluminescence, which suggests that faulting occurred under essentially diagenetic conditions (Knipe and Lloyd, 1994). Many grains also exhibit complex intragranular microstructures. Some of these microstructures are inherited from a pre-depositional history, but some exhibit contributions from the local effects of faulting. The latter microstructures form the subject of this contribution.

2.2. Analytical techniques

This study has exploited recent advances in SEM technology that permit both imaging of microstructures and exact determination of crystallographic orientation via electron backscattered diffraction or EBSD (see Wilkinson and Hirsch, 1997; Prior et al., 1999, for recent reviews). EBSD analysis has two related components (Fig. 2), fore-scattered electron (FSE) orientation contrast images (Field, 1997) and electron backscatter patterns (EBSPs). The former provide microstructural images of the specimen, whilst the latter are unique for a particular crystal orientation. EBSPs are indexed using commercially available computer programs to provide a range of petrofabric information and diagrams. We have used the Channel + ICE© software (Schmidt and Olesen, 1989). As both FSE and EBSP images can be obtained simultaneously, there is a one-to-one comparison between microstructure and crystallography (Dingley and Randle, 1992). It is possible also to automate the EBSP indexing procedure such that the electron beam is traversed across a chosen area in a stepwise manner and the pattern produced at each point is collected and indexed (e.g. Fig. 3). From these data, computer-generated images of the microstructure can be produced, based on several different parameters. Here we have used (Figs. 3 and 5–7) crystal orientation (using all three Euler angles), EBSP 'band contrast' (in which regions of better pattern quality appear brighter), and EBSP 'pattern misfit' or mean angular deviation (MAD), a measure of how well the simulation matches the real pattern. However, care must be taken when processing these automated images, particularly where the indexing success rate is poor (e.g. due to grain boundaries, cracks, voids, inclusions, dislocations, or specimen surface damage, etc.). Such 'zero solutions' can be removed by either 'extrapolation' of successful indexing results for adjacent points, or 'spike' correction of an individual measurement point with a wrong indexing solution relative to its neighbours. Such image-processing techniques may result in the production of false or exaggerated microstructures and/or crystal orientation components. It is important therefore not only to understand the effects of EBSD image processing but also to clearly state all image and crystal processing factors.

A further potential problem in EBSD analysis, with critical implications for this study, concerns the tendency to misindex EBSPs due to the existence of rotational symmetry elements, so-called pseudo-symmetry (e.g. Prior et al., 1999). This results in similar EBSPs for different orientations. The ***c***-axis in quartz is a pseudo-symmetry axis and 60° or 180° rotations produce similar EBSPs (e.g. Fig. 2). Unfortunately, the same rotation occurs in dauphiné twinning. The

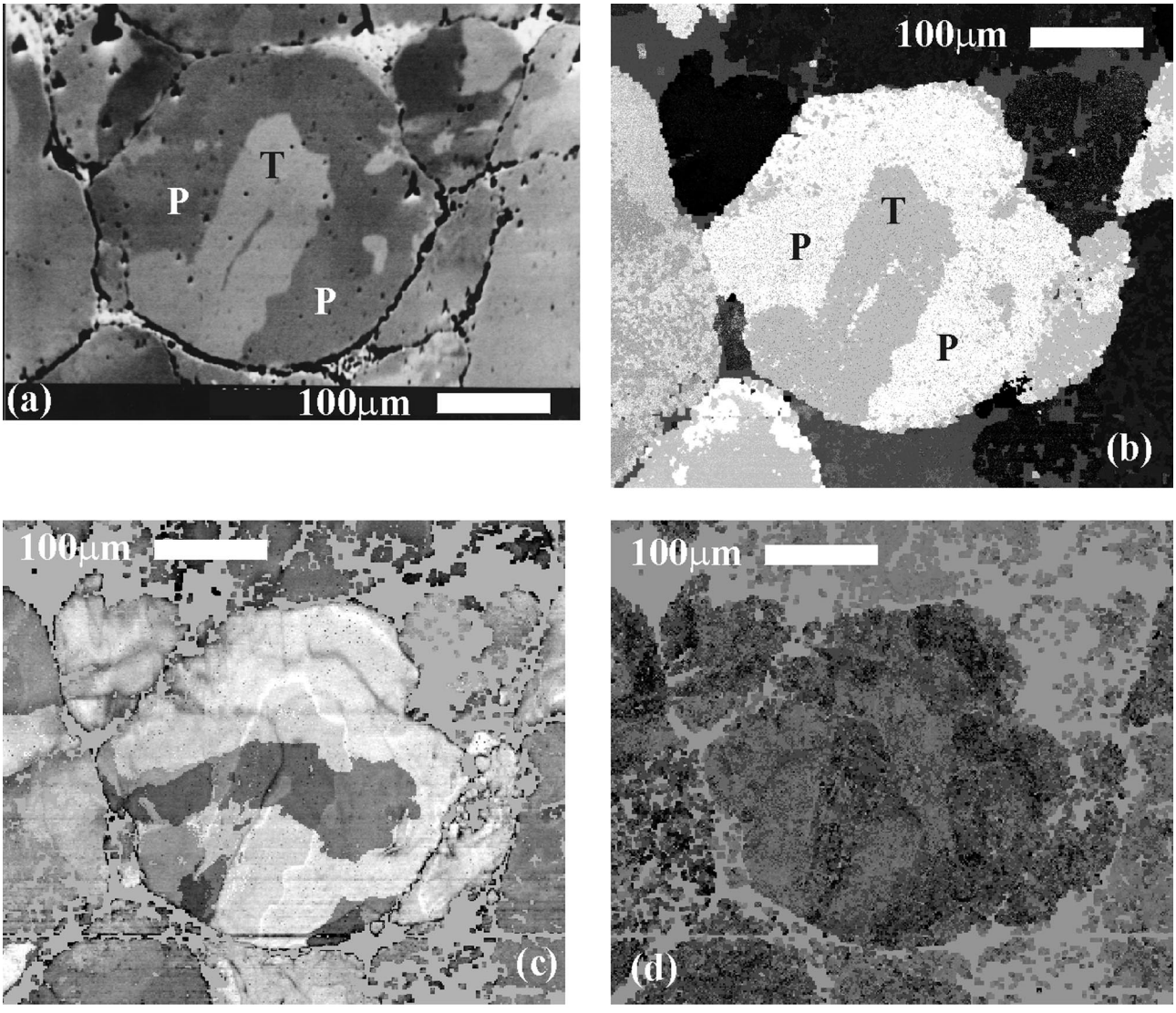

Fig. 3. Example of automatic SEM/EBSD analysis. Image processing details: 1 μm step procedure (330 × 339 = 125 430 steps), 1 spike removal and zero solution extrapolation; uniform light grey backgrounds in (b)–(d) indicate regions of zero EBSP solutions. (a) FSE microstructure; note subgrains. Manually derived EBSPs indicate a dauphiné twin relationship between regions P (parent) and T (twin). (b) Synthetic microstructural image based on all three Euler angles. (c) EBSP 'band contrast' (BC) image; note twin boundary indicated by white line and the region of darker BC contrast. (d) EBSP 'pattern misfit' (MAD) image; note 'subgrains'.

possibility exists therefore of confusing dauphiné twinning with pseudo-symmetry or vice versa, although fortunately the magnitude of rotation involved means that additional problems with measuring rotation angles for small angular misorientations (Prior, 1999) are not encountered. To prevent such mistakes, careful attention was given to all manually derived EBSPs, particularly the subtle background structure and the presence or absence of second order Bragg diffraction lines (e.g. Fig. 2). In addition, prior to automatic indexing experiments, the FSE image was assessed via manual EBSP analysis to identify the crystal orientations of the main microstructural elements and to ensure the validity of the automatic indexing procedure. It was found that reducing contrast in the EBSP images facilitated accurate automatic indexing and reduced significantly any potential pseudo-symmetry problems. The accurate simulation of real microstructures (e.g. Fig. 3) testifies to the veracity of this approach.

The general SEM operating parameters used in this study were as follows: tungsten filament and 20 keV accelerating voltage; ~20 nA specimen current; 70° specimen tilt angle. All samples were prepared according to the technique described by Lloyd (1987). The samples were then coated with a thin layer of carbon, deposited by vacuum evaporation, to prevent charging. However, towards the end of the study it was realised that by using a specimen tilt angle of ≥75° it was possible to examine uncoated samples using the same accelerating voltage and specimen current values without encountering specimen charging and hence image stability problems (e.g. Fig. 2). This is

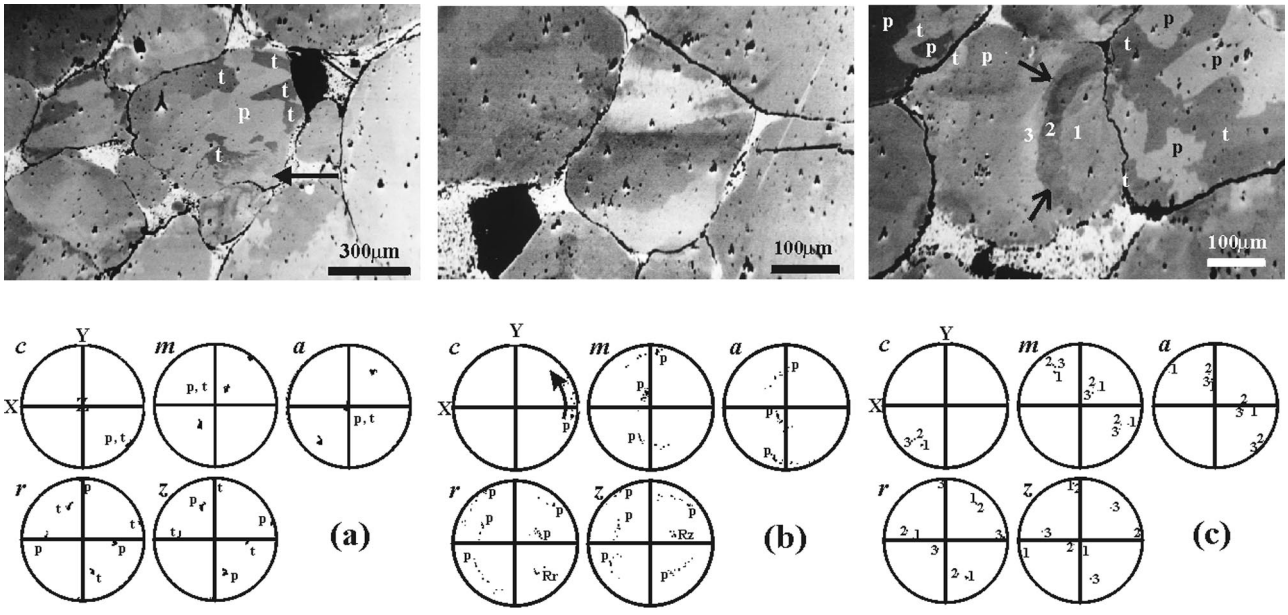

Fig. 4. SEM/EBSD examples of intragranular microstructures: *Above*, FSE image; *Below*, EBSP derived pole figures. (a) Dauphiné twinning microstructures (t) penetrate from grain contacts into the parental grain (p); note the exchange of ***r*** and ***z*** orientations. An arcuate zone of diffuse FSE contrast overprinting some twins is also visible (arrow—see Fig. 7). (b) Crystal slip microstructures due to changing crystal orientation, revealed by dispersion (arrowed for ***c***-axis) of individual crystal directions from original parental orientations (p). Clusters at R_r and R_z suggest that slip occurred on acute rhomb [±π](***a***) systems. (c) Progressive indentation microstructures. Parental (p) grains (right and upper left) have undergone dauphiné twinning (t), whilst the central grain exhibits both dauphiné twinning and an 'arcuate' deformation zone (arrowed), in which positions 1 and 2 have similar orientations and a dauphiné twinning relationship with position 3.

due to the fact that at high angles of tilt the electron flux entering the sample is less than that leaving the sample (Goldstein et al., 1992).

2.3. Dauphiné twinning

Further consideration of the occurrence of dauphiné twinning in quartz appears apposite because of the relationship between pseudo-symmetry and dauphiné twinning. According to Frondel (1962), twinning is the rule rather than the exception in quartz, with dauphiné twinning being by far the most common twin law observed. A precise description of dauphiné twinning requires the determination of the angular relationship between the axial systems of the twin components, the relationship between the polarity of the ***a***-axes, and the hand of the crystal (Frondel, 1962). However, because dauphiné twinning involves a 180° (or apparent 60°) rotation about ***c***, the orientation of ***c***, ***m*** and ***a*** remains constant. Thus, recognition of dauphiné twinning in quartz grains (rather than individual crystals) is very difficult and none can be recognised in thin-section via traditional optical means using the polarising microscope (e.g. Nicolas and Poirier, 1976). Fortunately, dauphiné twinning interchanges the ***r*** and ***z*** rhomb directions and this is easily distinguished via SEM/EBSD (e.g. Figs. 3 and 4).

Although several processes can cause dauphiné twinning (Frondel, 1962), applied local pressure at room temperature or higher and pure bending or torsion at temperatures from 573° to at least 300°C attest to a potential relationship with deformation. Dauphiné twinning also occurs on inversion from β to α quartz on cooling (Putnis, 1992; Nord, 1994). The extent of dauphiné twinning increases with the magnitude and duration of the local pressures, whilst the pressure necessary to induce twinning decreases as temperature increases. Each crystallographic surface has a characteristic minimum load and duration necessary to induce twinning; the ***m*** and ***a*** planes require less pressure and/or shorter duration than ***c*** planes. These observations suggest that dauphiné twinning probably represents an example of piezocrescence (Frondel, 1962), or a change in atomic positions due to the application of stress, and hence it should be common in deformed rocks. All atomic movements are small, do not break Si–O bonds, and result in only a slight difference in bond angles across the composition surface of the twin. Thus, the effect of applied stress is to cause movement of the translation zone at the twin boundary in such direction as to bring the crystal structure into equilibrium with the new stress system (e.g. Putnis, 1992). This operation involves a localised shear and the development of a narrow zone with an incommensurate (i.e. neither trigonal α, nor hexagonal β) quartz structure.

This brief discussion of dauphiné twinning suggests that it should be a common feature in quartz tectonites. However, because of its invisibility under traditional optical investigation, it remains ambiguous, with few reported observations (e.g. Thomas and Wooster, 1951; Tullis, 1970, 1971, 1980; Green et al., 1970; Tullis and Tullis, 1972; Baker and Wenk, 1972; Baker and Riekels, 1977;

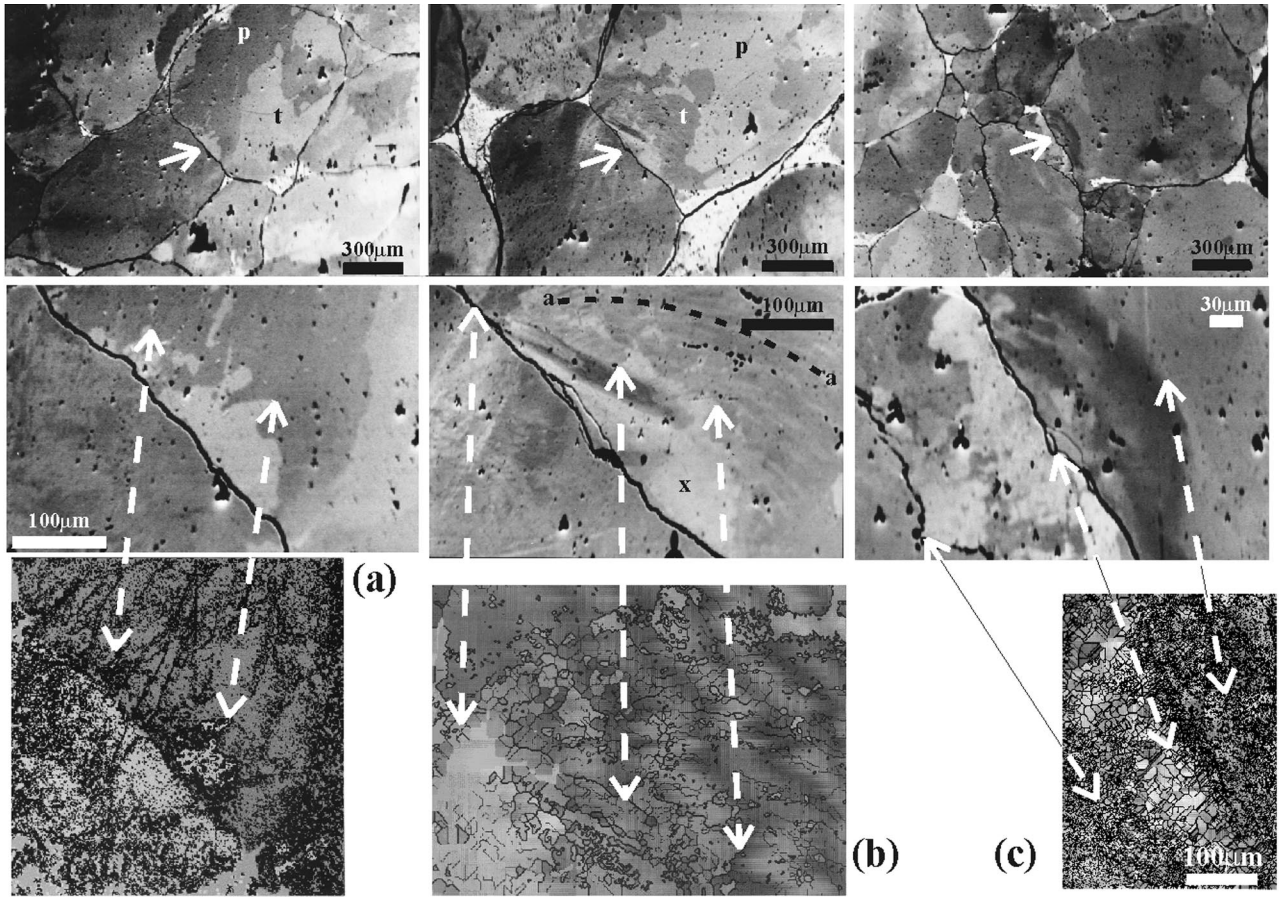

Fig. 5. Automatic SEM/EBSD examples of overprinting microstructures due to grain indentation: *upper*, FSE image; *centre*, FSE image detail; *lower*, automatic EBSD image (1 μm step procedure; black lines, <0.5° misoriented intragranular boundaries; uniform light grey backgrounds indicate regions of zero EBSP solutions). (a) Dauphiné twinning microstructures (p, parent; t, twin); single spike removal and extrapolation. (b) Incipient arcuate deformation zone (arrow, top; a–a, centre), overprinted by a later feature (x); single spike removal, three extrapolations. (c) Well-developed arcuate deformation zone (arrowed) and fine-scale 'subgrain' microstructure; single spike removal, three extrapolations.

Farmer, 1992; Neumann, 1996). The development of SEM/EBSD techniques perhaps allows for the first time the true recognition of the role of dauphiné twinning in quartz deformation.

3. Microstructural observations

There have been numerous studies of the behaviour of sandstones and quartzites during faulting (e.g. Gallagher et al., 1974; Aydin, 1978; Underhill and Woodcock, 1987; Blenkinsop and Drury, 1988; Aydin and Johnson, 1993; Hirth and Tullis, 1994; Menendez et al., 1996; Wong et al., 1997). Attention has concentrated on intragranular fracture and cataclastic microstructures, perhaps most clearly revealed by cathodoluminescence microscopy (e.g. Blenkinsop and Rutter, 1986; Lloyd and Knipe, 1992; Knipe and Lloyd, 1994). In this contribution, SEM/EBSD analysis has been used to observe distinct LTP and associated microstructures in quartz grains within the Skiag Bridge fault zone. As almost all grains present in the samples studied contain examples of these microstructures, this suggests that they are characteristic of the low-temperature deformation of quartz. However, it is not immediately clear whether they developed at the onset of deformation, prior to the establishment of a through-going fault plane, or are later features that developed within the damage zone remote from the main displacement segment. These microstructures are now described in terms of their apparent sequence of development.

3.1. LTP microstructures

3.1.1. Dauphiné twinning microstructures

Dauphiné twinning microstructures (e.g. Figs. 2–6) exhibit distinct and sharp changes in FSE contrast relative to that of the 'parent' grain and tend usually to emanate from a region of contact with a neighbouring grain. These features therefore have the appearance of classic penetration twins. EBSP analysis typically reveals no change in the ***c***, ***m*** and ***a*** crystal directions, but the characteristic swapping of the ***r*** and ***z*** indicative of 180° (i.e. 60°) rotation about the ***c***-axis common to all dauphiné twinning operations (e.g. Fig. 4a). This behaviour is shown by numerous (>50%?) quartz

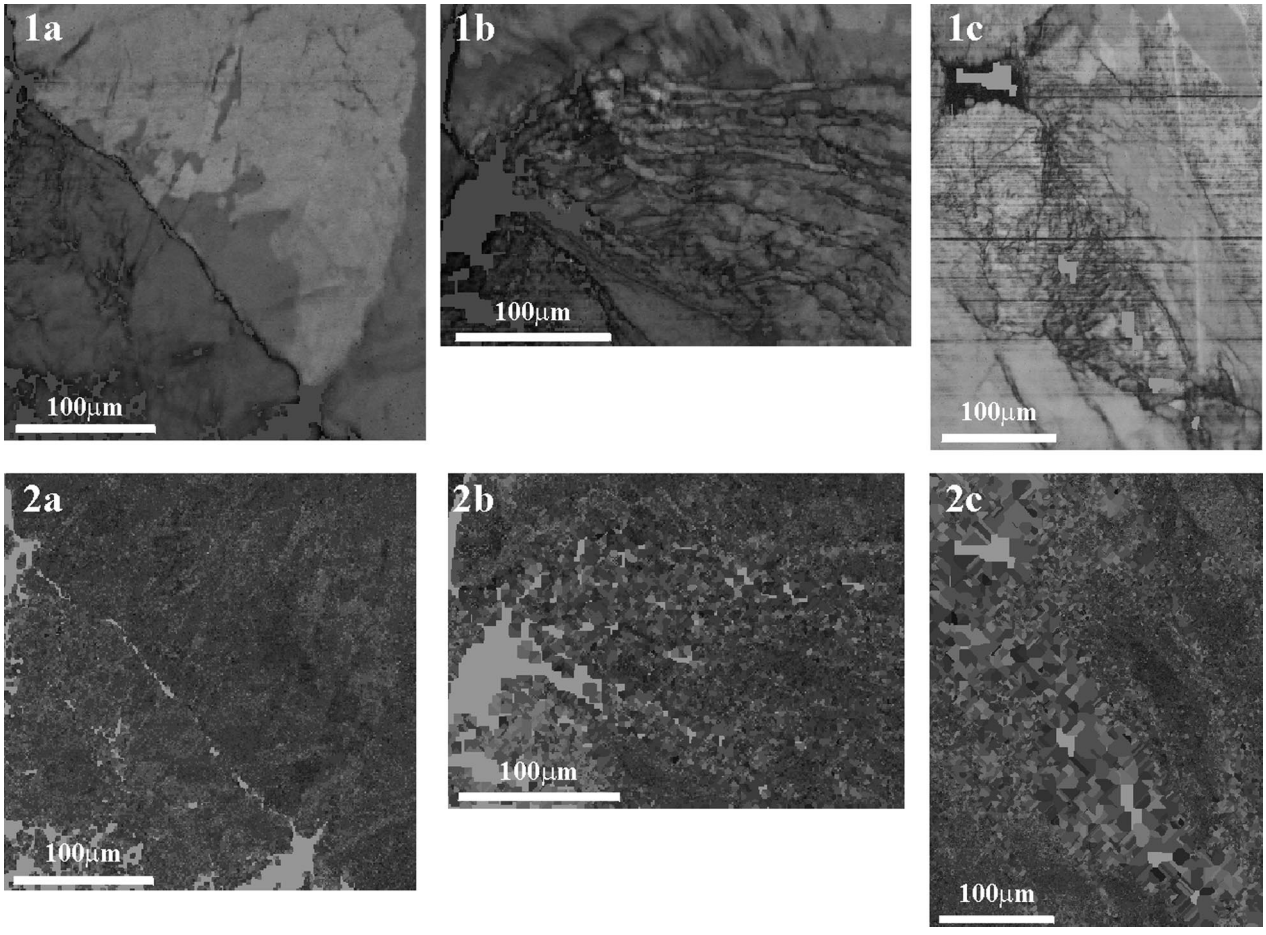

Fig. 6. Examples of image processed automatic EBSD grain indentation microstructures shown in Fig. 5a–c respectively: 1. band contrast (BC); 2. pattern misfit (MAD). Uniform light grey backgrounds indicate regions of zero EBSP solutions. (a) Dauphiné twinning microstructures. (b) Incipient arcuate deformation zone. (c) Well-developed arcuate deformation zone and fine-scale 'subgrain' microstructures.

grains in the wake zone to the Skiag Bridge fault. As many of these twins originate at contact points with adjacent grains, they appear to originate as a result of stress concentrations (i.e. 'piezocrescence') and grain indentation during faulting. However, it must be conceded that some proportion of the twins has been inherited prior to faulting. It is difficult to distinguish pre-faulting dauphiné twins but those examples apparently unrelated to grain contacts are the most likely candidates, although they may be due also to twins that originated out of the plane of section but which have grown to intersect the section plane.

3.1.2. Crystal slip microstructures

Crystal slip microstructures exhibit gradual variations in intragranular FSE contrast indicative of progressive change in crystal orientation (e.g. Figs. 2–5). They are analogous to the 'flame structures' described from these samples via optical microscopy (Lloyd and Knipe, 1992; Knipe and Lloyd, 1994). EBSP-derived pole figures typically show a dispersion of orientations from an original cluster that represents the parental grain orientation (e.g. Fig. 4b). However, not all crystal directions show dispersion and some remain as tight clusters. These represent 'rotation axes' that are unique for a specific crystal slip system (Lloyd and Freeman, 1991, 1994). In effect, the original crystal lattice of the parental grain has been bent around this rotation axis to form elongate or polygonised subgrains and/or deformation lamellae (e.g. Drury, 1993). In the example shown in Fig. 3, a darker region is observed in the band contrast image across the centre of the grain, which implies a zone of poorer EBSP quality. This is consistent with a bending of the crystal lattice due to the same indentation that produced the large dauphiné twin. However, this lattice bending 'overprints' the dauphiné twin. In addition, both FSE and pattern misfit (MAD) images reveal distinct intragranular regions with different contrasts and therefore interpreted as 'subgrains', which overprint the dauphiné twin and also 'distort' the twin boundary. Thus, although crystal slip microstructures are clearly another example of LTP induced by stress concentrations at grain contacts, they not only originate contemporaneously with, but also continue after dauphiné twinning. Furthermore, deformation is most intense at the point of indentation and diminishes progressively into grain. It should be possible therefore to observe microstructures

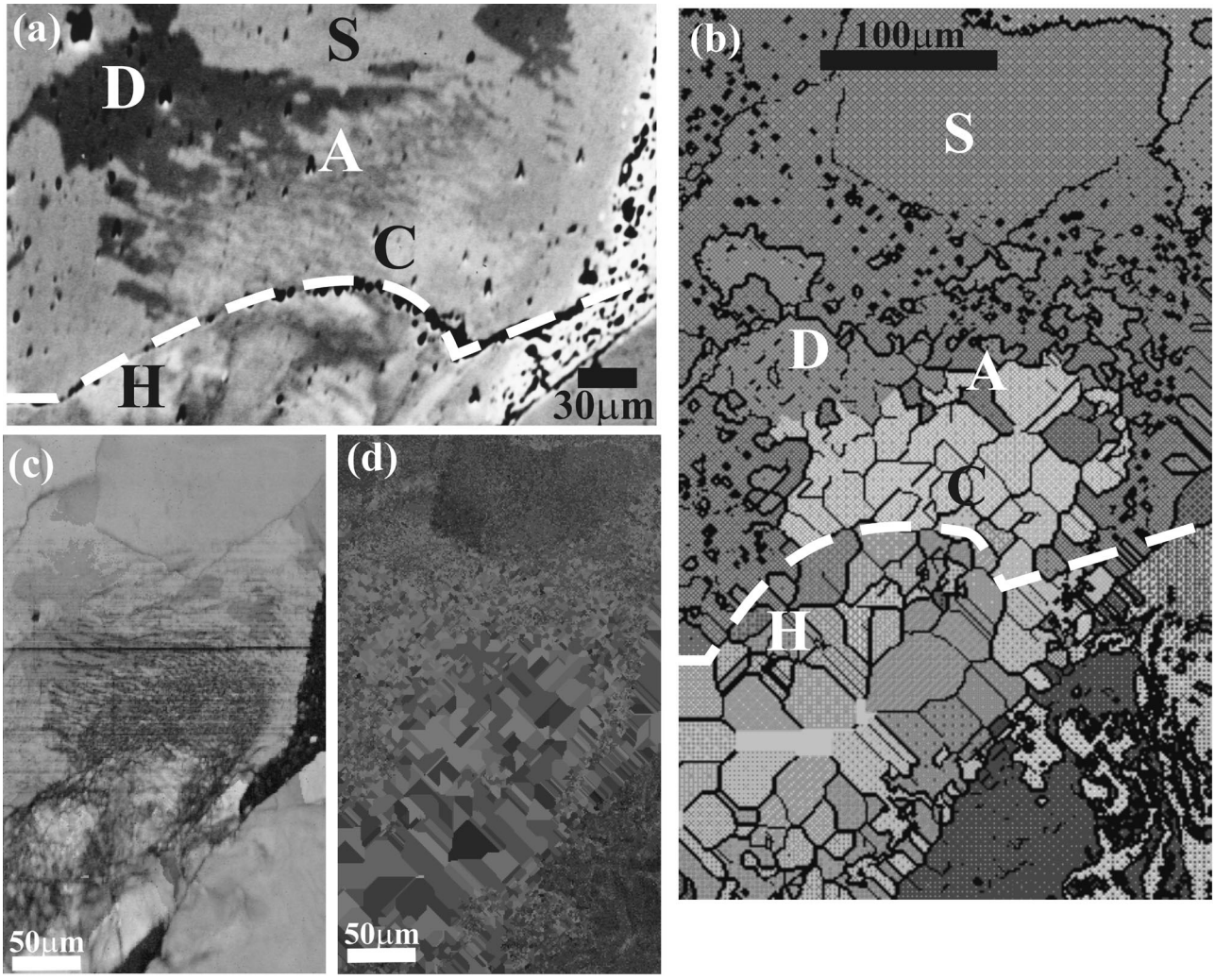

Fig. 7. Example of automatic SEM/EBSD analysis of progressive deformation (compare with Fig. 4a, arrow). Indentation of a 'soft' grain (S) by a 'hard' grain (H) results progressively in dauphiné twinning (D), then an arcuate subgrain array (A), and finally a region of high crystal orientation contrast (C). Processing details: single spike removal and three extrapolations due to poor EBSP resolution, resulting in some unrealistic 'subgrains'; uniform light grey backgrounds in (b)–(d) indicate regions of zero EBSP solutions. (a) FSE image. (b) Automatic SEM/EBSD simulation ($<10°$ misoriented subgrain boundaries indicated). (c) Band contrast image. (d) Pattern misfit (MAD) image.

that define the progressive nature of grain indentation deformation.

3.1.3. Progressive indentation microstructures

Progressive indentation microstructures are typically zones of 'arcuate' deformation and changing FSE contrast centred on contacts with neighbouring grains (e.g. Figs. 4–6). They have the appearance therefore of a deformation or 'indentation front' spreading out from the contact. The indentation front often has a dauphiné twin relationship (Fig. 4c) with the grain region on its convex side (i.e. 'ahead' of it). In contrast, it forms a diffuse low angle misorientation with the region of grain on its concave side (i.e. 'behind' it). This suggests that the arcuate indentation zone formed as a dauphiné twin at the point of grain contact and then migrated into the parental grain, diverging from the contact, whilst continued deformation behind the 'front' occurred via crystal slip processes. The indenting grain usually exhibits only the dauphiné twinning and/or crystal slip microstructures associated with the initial stages of indentation. This behaviour is consistent with the intuitive interpretation that the indenting grain should be harder than the indented grain and hence should show more resistance to deformation. Thus, arcuate deformation zones represent an instantaneous relic of the intergranular contact and indentation process. They consist of an undeformed 'foreland' ahead of an 'active' deformation front, behind which is a 'wake' zone of minor strain readjustments. This visualisation emphasises the progressive nature of indentation deformation. Further support is provided by various overprinting relationships that exist between the LTP microstructures so far described. Fig. 4a contains a zone of deformation at the point of grain contact that overprints an earlier formed

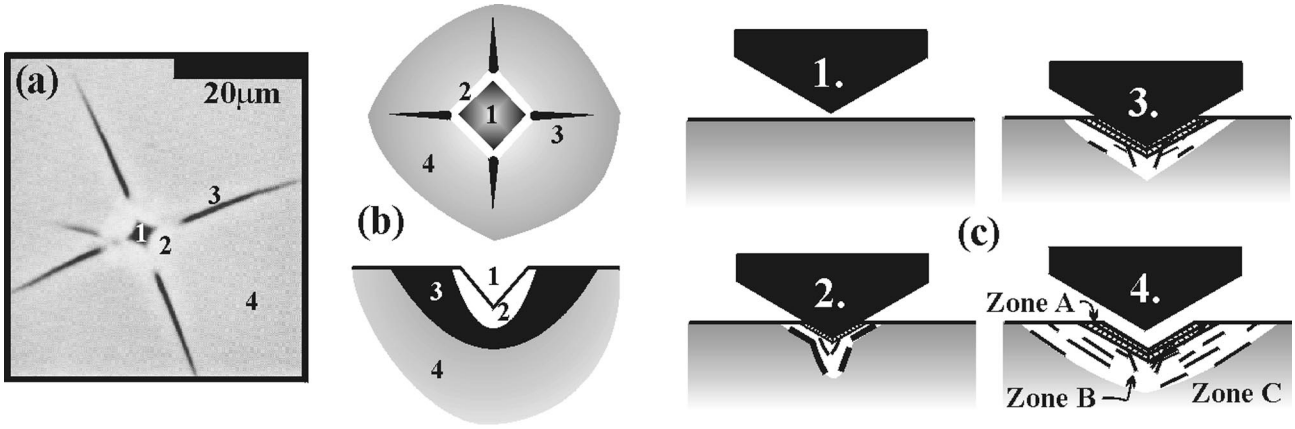

Fig. 8. Summary of Vickers microhardness indentation tests of quartz, based on SEM and TEM observations (after Ferguson et al., 1987). (a) BSE image after some serial sectioning (1, indenter impression; 2, high BSE contrast region; 3, median–radial cracks; 4, undamaged quartz). (b) Schematic plan (above) and section (below) views (1–4 as above). (c) Schematic microstructural evolution during indenter impression (1–3) and release (4): A, intensely deformed region of high fracture density and cryptocrystallinity; B, less deformed region of lower fracture density; C, undamaged quartz with median cracks.

dauphiné twin. Similar features are revealed via automated SEM/EBSD analysis of other fine-scale grain indentation microstructures (e.g. Figs. 5–7).

3.2. Microstructural evolution

The examples described above clearly show the progressive development and superposition of microstructures due to intergranular indentation. Initial indentation causes dauphiné twinning (Fig. 5a) and subsequent overprinting twinning events can occur with continued indentation (Fig. 6a). The later stages of twinning are frequently associated with the formation of incipient subgrain microstructures and very small (i.e. $<0.5°$) misorientations (Figs. 5–7). Continued indentation results in formation of an incipient arcuate deformation zone or indentation front consisting of an arcuate array of subgrains (e.g. Figs. 5b,c and 6b,c), which overprints the dauphiné twins. The development of concentric strain fronts is evidently possible (Fig. 6b,c). Subsequently, a feature with high FSE reflectance (contrast) characteristics but poor EBSP resolution overprints both the dauphiné twinning and arcuate subgrain array LTP microstructures (e.g. Fig. 7). The origin of this feature is central to understanding and explaining grain indentation processes.

4. A model for grain indentation

4.1. Previous results

Further explanation for grain contact indentation processes is provided by SEM/transmission electron microscopic (TEM) analysis of quartz crystals used for Vickers microhardness tests (Ferguson et al., 1987). Indentation caused an intensely deformed region to develop beneath the indenter (Fig. 8a,b). This region exhibited high backscattered electron (BSE) reflectance or contrast (HCR) but poor or zero BSE electron diffraction characteristics (Fig. 8a) when imaged via SEM electron channelling techniques (e.g. Lloyd, 1987; Lloyd et al., 1991). These BSE characteristics are identical to the FSE and EBSP observations reported in the previous section. Removal of surface material by serial sectioning revealed that the median–radial cracks due to indentation do not penetrate the high contrast region at depth.

Ferguson et al. (1987) further analysed the microstructure of the HCR region via TEM. This revealed a high density of microfractures, possibly involving some partial melting and glass formation, and a submicron scale ‘blocky’ microstructure. Thus, microfracturing largely eliminated the need for any ‘plastic’ deformation, although the absence of voids implied some strain accommodation via LTP. Deformation mechanisms and associated microstructures developed sequentially as indentation progressed. Significantly, the microstructure continued to evolve during stress relaxation, as the indenter was withdrawn.

Based on these observations, Ferguson et al. (1987) proposed the following model for microhardness indentation (Fig. 8c). Progressive indentation (steps 1–3) causes an intensely deformed region to develop (zone A) with high fracture density that forms ‘tilt-blocks’ and a cryptocrystalline microstructure. A less deformed region (zone B) surrounds this with lower fracture density and some indication of plastic deformation. Zone B is surrounded by essentially undamaged quartz (zone C) traversed by the propagation of median–radial cracks. All three zones continue to evolve microstructurally during indenter release, as revealed by cross-cutting microfractures (step 4).

4.2. Grain indentation model

These observations on and the model for microhardness indentation processes are not only compatible with the grain boundary contact and indentation microstructures described above but are crucial to their explanation. The

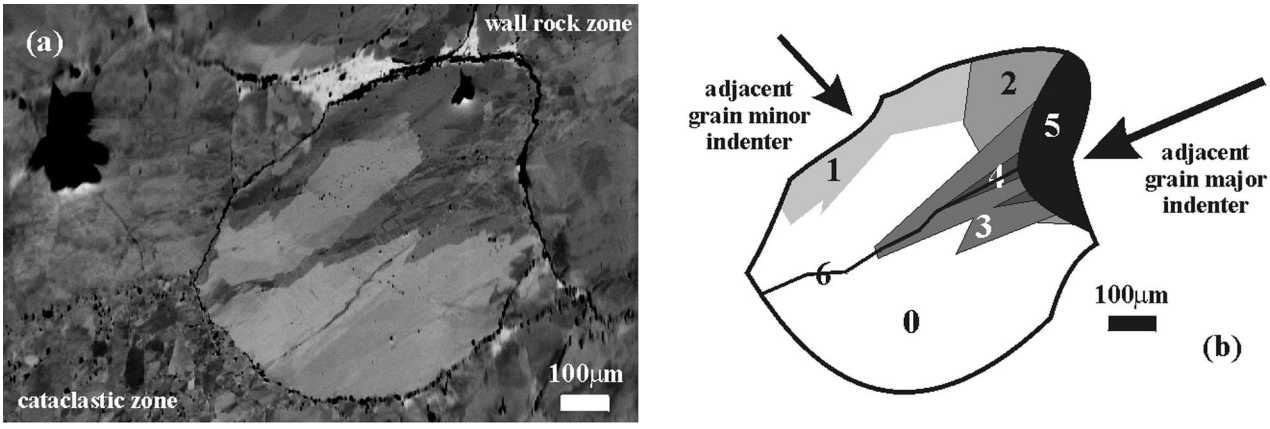

Fig. 9. Summary of progressive grain indentation and microstructural superposition. (a) Uncoated FSE image of intragranular microstructure. (b) Schematic interpretation: 0, original parental grain; 1 and 2, initial penetration dauphiné twins; 3 and 4, subsequent overprinting penetration twinning; 5, fine-scale 'subgrains; and 6, LTP microstructure and/or transgranular microcrack.

microhardness indenter model illustrated in Fig. 8 can be represented in terms of intergrain indentation as follows (see Fig. 9). An original parental grain can be indented by any neighbouring grain, or might act as an indenter itself. These initial indentation microstructures share dauphiné twin relationships with the parent grain. Multiple indenters exhibit overprinting dauphiné twinning relationships, with perhaps one indenter direction eventually dominating. As indentation continues and dauphiné twins penetrate further into the parent grain, they are progressively overprinted from the indenter contact by fine-scale arcuate microstructural arrays. These consist of either subgrains due to LTP, or cellular 'fault block' networks due to microfracturing. Indeed, by analogy with microhardness indentation, the high FSE contrast but poor EBSP resolution feature that subsequently overprints dauphiné twin and arcuate subgrain microstructures (e.g. Fig. 7) represents a pervasive and penetrative cold-worked, strain-hardened region that may provide sites for microfracture nucleation. Finally, a narrow region of LTP deformation develops from these regions right across the grain. The strain hardening associated with this is capable of nucleating a transgranular microcrack and hence the initiation of cataclasis. This microstructural evolution can be observed either in part or totally in many grains from the wake zone to the Skiag Bridge fault, particularly those close to the through-going cataclastic zones (e.g. Fig. 9).

5. Significance of dauphiné twinning

The recognition of dauphiné twinning is becoming increasingly common with the use of SEM/EBSD (e.g. Olesen and Schmidt, 1990; Lloyd and Freeman, 1991, 1994; Lloyd et al., 1992, 1997; Mainprice et al., 1993; Fliervoet and White, 1995; Trimby et al., 1998; Fliervoet et al., 1999; Trimby and Prior, 1999). It has been recognised in a range of geological environments from diagenetic to amphibolite facies conditions, consistent with Frondel's (1962) original assertions. Nevertheless, the significance of dauphiné twinning in quartz has been the subject of considerable discussion (e.g. Barber and Wenk, 1991). Dauphiné twinning is a form of LTP involving a specific crystallographic transformation due to resolved shear stress that accomplishes only a limited amount of strain. It might be used therefore to infer stress orientations (Turner, 1962), strain magnitudes in weakly deformed rocks (Groshong et al., 1984) and perhaps stress magnitudes (Tullis, 1980). Thus, because dauphiné twinning is found to be a common microstructure of the Skiag Bridge fault zone, it represents potentially a unique record of the early and/or low stress/strain history and in particular the stress concentration history at grain contacts. In this section, the results described above are considered in terms of the significance of dauphiné twinning for deformation mechanisms and microstructural evolution. Although these results were obtained from a study of cataclastic fault rocks, they have implications for all quartz tectonites.

5.1. Petrophysical background

To evaluate the significance of dauphiné twinning requires knowledge of the elastic constants of quartz. These were calculated for the single crystal by McSkimin et al. (1965). Although they did not state the 'hand' of the crystal, this is not vital, as elastic properties are centrosymmetric. Thus, a traditional right-handed helix has been assumed (e.g. Mainprice et al., 1993). The parameters of interest are variations in Young's modulus, uniaxial compliance (S_{1111}), linear compressibility and seismic P-wave velocity (Mainprice, pers. comm., 1999; see Fig. 10a). Although the maximum in Young's modulus (1.30 Mb) and hence minimum in compliance (0.77 Mb^{-1}) are parallel to the *z* rhombs, the minimum in Young's modulus (0.96 Mb) and maximum in compliance (1.45 Mb^{-1}) are offset slightly from the ***r*** rhombs to lie between the ***r*** and ***m***

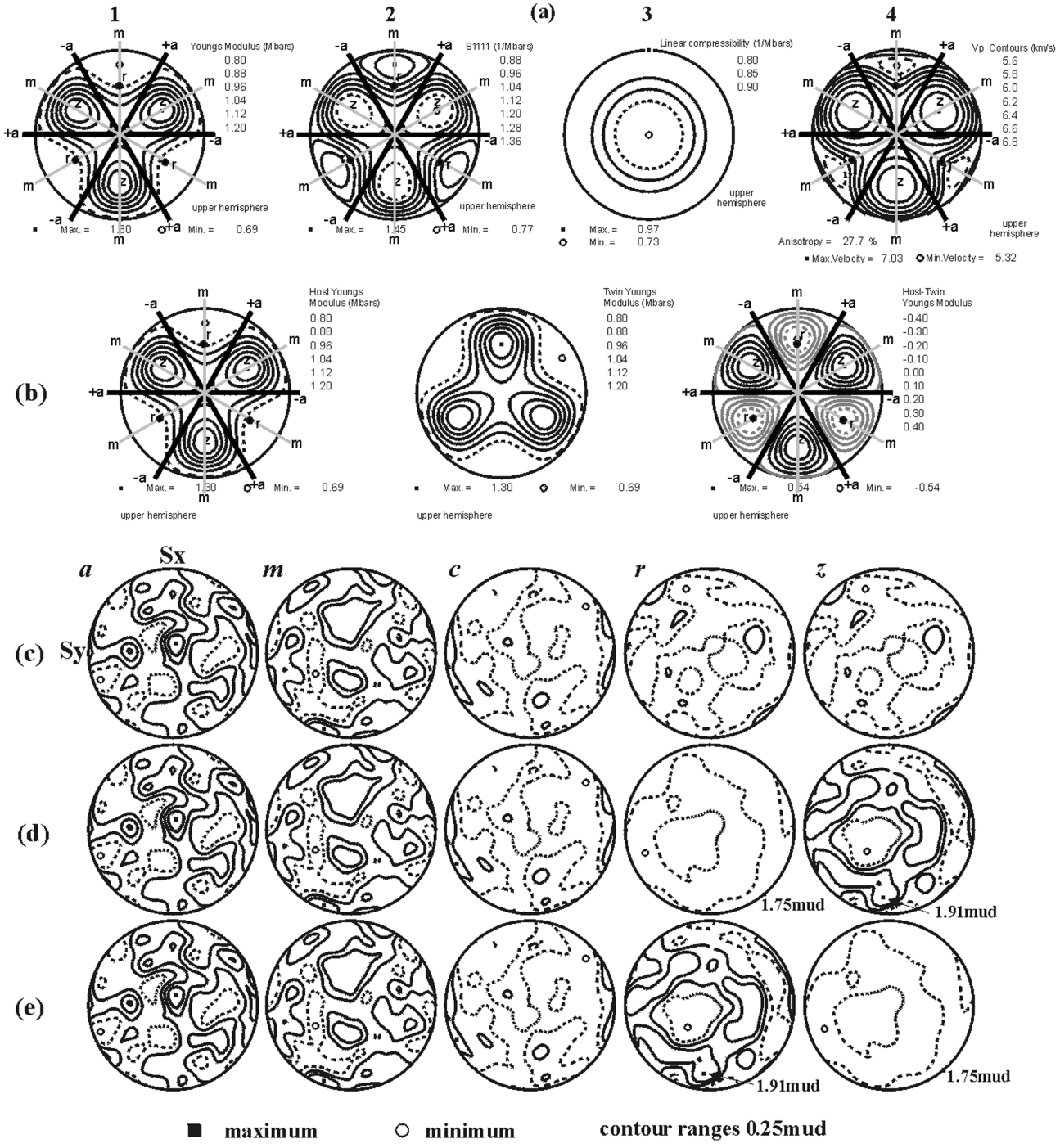

Fig. 10. Dauphiné twinning and petrofabric analysis (N.B. petrofabrics have been measured in sample coordinates, S_X, S_Y, S_Z; see Fig. 11). (a) Variations in physical properties (Mainprice, pers. comm., 1999), determined from quartz single crystal elastic constants (McSkimin et al., 1965): 1, Young's modulus; 2, uniaxial compliance (S_{1111}); 3, linear compressibility; 4, seismic P wave velocity. (b) Comparison of Young's modulus variation for host (left) and twin (centre) regions of a parent grain (Mainprice, pers. comm., 1999). In the 'combined' distribution (right), positive values (black) should twin whilst negative values (grey) should not twin. (c) 50% parent and 50% dauphiné twin petrofabric. (d) 100% parent petrofabric. (e) 100% dauphiné twin petrofabric.

directions. The minimum in linear compressibility (0.73 Mb^{-1}) is parallel to the ***c***-axis and the maximum (0.97 Mb^{-1}) lies symmetrically within the basal plane. The minimum compliance corresponds to the maximum stiffness, which should be close therefore to the maximum in V_p. Thus, V_p-max (7.03 $km.s^{-1}$) is predicted to be parallel to the ***z*** rhombs (see also Mainprice et al., 1993), with V_p-min (5.32 $km.s^{-1}$) between the ***r*** and ***m*** directions, resulting in a single crystal V_p seismic anisotropy of 27.7%.

It is possible to predict the behaviour of a polycrystal aggregate from the single crystal elastic constant data if the petrofabric is known (e.g. Mainprice et al., 1993;

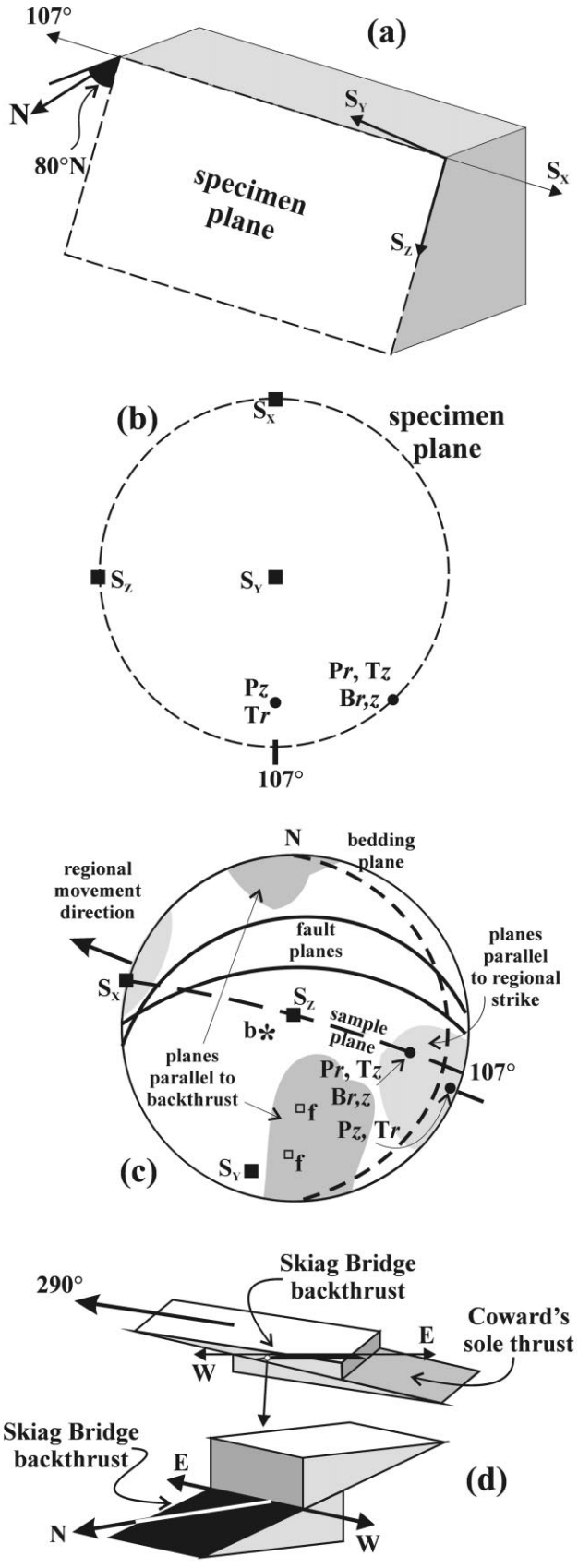

Fig. 11. Relationship between sample and geographical/field coordinate systems. (a) Sample (4)7139A coordinate system (S_X, S_Y, S_Z). (b) Representation of ***r*** and ***z*** petrofabric maxima orientations in sample coordinates (P, parent; T, dauphiné twin; B, parent-plus-twin). (c) Geographical representation of sample coordinate system, ***r*** and ***z*** petrofabric maxima, and (after Knipe and Lloyd, 1994) planes parallel to the regional strike and the local back thrust, fault planes (f) and bedding (b). (d) Schematic representation of, and relationship between, Coward's 'Sole' thrust and the Skiag Bridge back thrust or oblique ramp (black ornament).

Mainprice and Humbert, 1994; Lapierre et al., 1996). This in turn should provide insight into the potential significance of dauphiné twinning. The following approach has been adopted. EBSPs were measured for 250 grains chosen at random in sample 7139A of Knipe and Lloyd (1994), located in the hanging wall ~4 m from the main movement plane of the Skiag Bridge fault (Fig. 11a). To negate selection of a dauphiné twin orientation, the patterns were obtained from the centre of each grain avoiding any obvious twinned regions in the FSE image. This is regarded therefore as the original or parental petrofabric (Fig. 10d). However, many grains do contain dauphiné twins and their impact has not been included in this petrofabric. Fortunately, it is relatively easy to incorporate a dauphiné twin component by simply applying to each parental grain orientation determination the quartz pseudo-symmetry operator contained within the EBSD pattern recognition software (Fig. 10e). This operator leaves the ***c***, ***m*** and ***a*** pole figures unchanged but interchanges those for ***r*** and ***z***. The effect of dauphiné twinning on the bulk petrofabric can be gauged by combining the two fabrics, although this does assume that the bulk petrofabric contains 50% parent and 50% dauphiné twin orientations by volume (Fig. 10c). This approach provides therefore the midpoint between 100% parent (Fig. 10d) and 100% twin (Fig. 10e) petrofabrics.

The parental petrofabrics for the main crystal directions are very weak and can be considered as essentially random (Fig. 10d), although the ***r*** and ***z*** fabrics are not exactly equivalent as their maximum values are 1.73 mud and 1.91 mud, respectively. They are particularly suitable therefore for observing the effect of dauphiné twinning because all possible directions in orientation space are sampled and hence any tendency to twin should be recorded. The implications of these petrofabrics in terms of the early and/or low stress/strain history and the significance of dauphiné twinning in general are now considered.

5.2. Compressive stress orientation

It has been suggested that dauphiné twinning in quartz produces an ***r*** fabric maximum subparallel to the maximum compression direction (Tullis, 1970, 1971; Green et al., 1970; Baker and Wenk, 1972; Tullis and Tullis, 1972; Baker and Riekels, 1977). As we have seen (Fig. 10a), ***r*** is close to the maximum compliance direction (see also Fig. 10b). The difference in elastic strain energy (δW) between a twinned crystal and its host is positive for all

orientations in the crystal sector bounded by ***a–m–z–c*** directions and negative for all orientations in the ***a–m–r–c*** sector for a uniaxial stress state (Tullis and Tullis, 1972). All orientations for which δW is positive should twin such that sector ***a–m–z–c*** becomes sector ***a–m–r–c*** (Fig. 10b). Thus, parent grains with the pole of ***z*** (sub)parallel to the maximum compressive stress direction will undergo dauphiné twinning to produce twins with the pole of ***r*** parallel to this direction. The maximum in the ***r*** pole figure should indicate therefore the maximum compression direction.

If we consider only the parental petrofabric (Fig. 10d), there is clearly no obvious maximum in ***r***. However, if we incorporate dauphiné twinning (Fig. 10e), a maximum becomes apparent, oriented ~N–S in the sample coordinate system (Fig. 11b), equivalent to the ***z*** fabric in the parent. These sample ***r*** maxima fabrics can be related to the geographical coordinate system and various field measurement data (Knipe and Lloyd, 1994) by a simple stereographic rotation (Fig. 11c). Both maxima fall within the region of 'normals-to-planes parallel to the regional tectonic strike', rather than the region of 'normals-to-planes parallel to the Skiag Bridge back thrust'. This orientation is compatible with the principal compressive direction for the regional (i.e. Moine Thrust Zone) deformation rather than the local (i.e. Skiag Bridge back thrust fault) deformation (Fig. 11d). Thus, regional rather than local deformation has caused the dauphiné twinning microstructures in this sample, which must occur therefore within the wake zone to the 'Sole Thrust' recognised by Coward (1984, 1985) and not the wake zone to the Skiag Bridge back thrust. Nevertheless, it does appear from this analysis that principal compressive stress orientations can be determined from quartz crystal pole figures, but only by careful consideration of the contribution to, and effect on, the overall fabric due to dauphiné twinning.

5.3. Seismic anisotropy

Owing to the relationship between maximum seismic P-wave velocity and minimum in compliance, or maximum in stiffness (Fig. 10a), quartz rocks with non-random ***z*** petrofabrics are likely to be seismically anisotropic. This observation may be significant in terms of geophysical interpretation of seismic surveys through quartz-rich rocks. Although the parental Pipe Rock Quartzite has random **c**, ***m***, ***a*** and ***r*** petrofabrics (Fig. 10d), the ***z*** fabric is non-random and shows a small circle distribution centred subparallel on the sample S_Y direction, with a maximum oriented ~N–S in sample coordinates (Fig. 11b). In geographical coordinates (Fig. 11c), S_Y is normal to the regional movement direction and is likely to indicate therefore the intermediate compressive stress direction for the regional deformation. Thus, the ***z*** fabric not only imparts a seismic anisotropy, with maximum close to the regional movement direction (i.e. tectonic X), but may also be used to indicate the intermediate stress orientation. However, the effects of dauphiné twinning clearly complicate this behaviour (Fig. 10c–e) by progressively rotating and diminishing the strength of the ***z*** fabric whilst concomitantly increasing the strength of the ***r*** fabric. This implies that dauphiné twinning acts to reduce seismic anisotropy in quartzites.

5.4. Anisotropy of fracture

Bloss (1957) showed that the anisotropy of fracture strength in quartz depends on crystal orientation. Ferguson et al. (1987) developed this approach to show that the mode I fracture toughness (K_{Ic}) for ***r***, ***m*** and ***c*** is 1.74, 2.14 and 2.40 $MNm^{-3/2}$, respectively. This variation probably reflects real differences in ultimate tensile strength for these crystallographic planes because the increase from ***r***-to-***m***-to-***c*** is exactly that predicted from the areal density of Si–O bonds (Frondel, 1962). Frondel further suggested that fracturing may be associated with or bordered by 'secondary' dauphiné twinning. This implies that dauphiné twinning influences the response of individual quartz grains to fracture, depending on the crystal orientation of the grain relative to the imposed stress–strain system. This is essentially the association observed in quartz grains from the Skiag Bridge fault zone, where intragranular fractures follow and/or exploit dauphiné twin boundaries (e.g. Fig. 9). Thus, it is possible that the ***r*** (and ***z***?) fabrics for twinning (Fig. 10e) and the whole rock (Fig. 10c) indicate the preferred orientation of sets of fracture planes. However, the question remains whether it is the twin boundary orientation (i.e. the local crystallography) and/or the change in bulk elastic constants that are important in this evaluation. This depends on the scale of observation, microscopic crystal or macroscopic polycrystal. From Fig. 11, it does appear that there is a relationship between the microscopic fabric and the macroscopic stress system.

5.5. Acoustic emission

The narrow zone of incommensurate quartz structure that develops during dauphiné twinning represents a vibrational mode of the hexagonal β quartz structure (Putnis, 1992). Dauphiné twinning therefore is likely to be a strong acoustic inhomogeneity associated with acoustic emissions (e.g. Gurtovoi and Eremenko, 1991). It is possible that some acoustic emissions detected during experimental deformation tests of sandstones and quartzites and attributed to microfracturing are actually due to dauphiné twinning (e.g. Schmidt-Mumm, 1991). Furthermore, Glover et al. (1995) reported high acoustic emission at the α–to–β quartz phase transformation superposed on a background noise due to thermal cracking. This emphasises the need to perform detailed SEM/EBSD microstructural analysis of experimental samples both before and after deformation to determine the level and role of dauphiné twinning induced during the experimental tests. Based on observations made in this contribution, it is suggested

that many dauphiné twins are induced during the earliest stages of deformation and are likely to provide the nucleation sites for subsequent intergranular microfractures.

5.6. Crystal plastic deformation

As we have seen (Fig. 10), dauphiné twinning has no overall effect on the ***a*** petrofabric. However, in detail it does change the polarity of the $\pm$ ***a*** directions and this may have important consequences for quartz crystal plastic deformation. It is known (e.g. Nicolas and Poirier, 1976; Linker et al., 1984; Hirth and Tullis, 1992) that ***a*** is the preferred slip direction for many quartz crystal slip systems (e.g. basal-***a***, rhomb-***a*** and prism-***a***). It has been suggested (e.g. Griggs et al., 1960) that slip may be easier (i.e. have a lower critical resolved shear stress) parallel to $-$***a*** compared with $+$***a***, although this has recently been refuted for calcite (De Bresser and Spiers, 1997). Thus, dauphiné twinning may aid crystal slip dominated deformation processes by rotating with very little effort the easier $-$***a*** slip direction by 60° towards the preferred bulk deformation direction (*X*). Furthermore, the microstructure can be continually 'refreshed' to assist progressive deformation and prevent strain hardening by repeated dauphiné twinning of the intragranular microstructure.

5.7. Dauphiné twin and CSL boundaries

Recently, Lloyd et al. (1997) hypothesised that boundaries are important elements in a microstructure. If dauphiné twinning is common in quartz tectonites, it must be responsible for building a large proportion of the boundaries that might evolve during deformation. Such boundaries comprise an incommensurate quartz structure (Putnis, 1992) and are built normal to the basal plane parallel to the ***c***-axis. Thus, they are pure tilt boundaries as the rotation axis is parallel to the boundary plane (Lloyd et al., 1997). Intragranular boundaries produced by mechanical twinning therefore may either hinder or enhance deformation by other mechanisms or processes (Rutter, 1995). Indeed, because dauphiné twinning is much more common than hitherto appreciated, it might provide an extra degree of freedom to facilitate homogeneous rock deformation (Snoke et al., 1998). In this respect, it is interesting to note that attempts to recognise coincident site lattice (CSL) boundaries have so far proved elusive (e.g. McLaren, 1986; Lind, 1996; Dingley, 1999). Such boundaries should in principle have low energy and possess important properties in terms of deformation. However, dauphiné twin boundaries are a form of CSL boundary with twin index $\Sigma = 1$. It is conceivable therefore that the tendency for quartz to form easily dauphiné twin boundaries assumes the role of CSL boundaries in quartz tectonites.

6. Deformation mechanisms and microstructural evolution

In this section, the implications of intergranular contact stress concentrations, including dauphiné twinning, are discussed in terms of quartz deformation mechanisms and the consequences for microstructural evolution in quartz tectonites. The use of SEM/EBSD analysis to observe the LTP microstructures that develop during the earliest and/or lowest stress stages of faulting (i.e. associated with either the process zone or the wake zone) has considerable implications for fault zone evolution. In this respect, three existing models due to Meike (1990), Gratz (1991) and Gratier et al. (1999) are particularly relevant. The Gratz model has been supported recently by den Brok (1998).

6.1. Previous models

The essential conclusions of the Meike (1990), Gratz (1991), and Gratier et al. (1999) models are as follows.

1. The greatest strain energy is obtained from free dislocations; free dislocation pile-ups favour dislocation enhanced selective dissolution, DESD (Meike).
2. Ductile deformation results in a decrease in the potential for DESD (Meike).
3. DESD and DMT occupy similar regions on deformation mechanism maps and may be difficult to distinguish microstructurally (Meike).
4. DESD is dependent on crystallographic orientation and provides the potential for heterogeneous and anisotropic texture development (Meike, Gratz).
5. The kinetics of DMT are inversely proportional to the diameter of the surface of dissolution (Gratier).
6. Grain boundaries have a static island–channel network structure, with channels located where microcracks intersect the boundary; the rate of material transport is governed by thin-film diffusion at the islands, analogous to stress corrosion microcracking, such that DMT deformation rates are sensitive to microcracking (Gratz, Gratier).
7. Sudden increases in stress or fluid pressure may lead to microcracking, resulting in orders of magnitude increase in DMT deformation rates (Gratz, Gratier); fracture occurs during DMT creep to regulate strain rate and stress levels with time (Gratier).
8. The mechanical behaviour of the crust integrates successive brittle (fast) incremental events and viscous (slow) deformation that are not independent (Gratier).

Not only are these three models consistent with the observations described in the present contribution, but the latter also provides a unifying explanation for the models. This in turn accounts for the commonly observed occurrence of significant DMT deformation in coarse-grained sandstones

and quartzites and the aseismic–seismic faulting cycle, as follows.

6.2. Comparison of models and EBSD results

The essential feature of the observations described in this contribution is the progressive microstructural evolution that occurs at grain boundary contacts due to stress concentration induced cold work hardening. Although cold work hardening initially involves the formation of perhaps several generations of dauphiné twins, it also generates free dislocations and dislocation pile-ups that evolve into dense tangles of dislocations as work hardening progresses (cf. Meike model). This creates a cellular network of apparently significantly reduced 'grain size' (cf. Ferguson et al., 1987), which enhances dissolution. Eventually, stress concentration and cold work hardening are sufficient to produce microfracturing that creates an island–channel network on the boundaries (cf. Gratz and Gratier models), further enhancing dissolution. Concomitantly, cold work hardening and stress levels increase and the former propagates into the interior of grains, which are progressively involved in the deformation. However, because these regions are isolated from the kinetic effects of the dislocation enhanced selective diffusion and island–channel networks that are restricted to grain boundary contacts, dauphiné twins, LTP and fracture dominate rather than pressure solution. This is consistent with the progressive 'spalling' of grain fragments into cataclastic zones (e.g. Lloyd and Knipe, 1992; Knipe and Lloyd, 1994).

6.3. DMT in coarse-grain quartz rocks

Deformation via DMT is a widely occurring feature of sandstones and quartzites deformed under non-metamorphic or low-grade conditions, irrespective of grain size (e.g. Rutter, 1983; Houseknecht, 1988). However, the classic constitutive equations for DMT processes include an inverse dependence on grain size (i.e. 'grain size sensitive creep') that should preclude these processes from coarse grain size rocks. The reason they can operate is because of the occurrence of stress concentrations and the development of localised cold worked microstructures via LTP and/or microfracturing at grain boundary contacts. These micron–submicron scale microstructures, whether consisting of a subgrain array or a microfracture-bounded cellular array, reduce the effective 'grain' size and hence diffusion path length to that required for DMT processes. They also develop the island–channel networks (i.e. Gratz and Gratier models) and concentrations of free dislocations (i.e. Meike model) that assist fluid effects and stress corrosion microfracturing, resulting in a self-regulating system. As material is removed from the boundary contact areas, the deformation front progresses further in to the grain and DMT continues, gradually 'dissolving' the grain away.

There are several other lines of supportive evidence for this explanation of DMT processes. Wheeler (1987) noted the significance of grain scale stresses in the kinetics of metamorphism, whilst Berka (1982) recognised stress concentrations along grain contacts. Wintsch and Dunning (1985) provided earlier support for the Meike model of DESD by acknowledging the effect of dislocation density on the aqueous solubility of quartz, which is obviously important with respect to the DMT process. In addition, various workers have noted the consequences for change in deformation mechanism by reducing grain size (e.g. Schneibel et al., 1981; Freeman and Ferguson, 1986; Houseknecht, 1984). However, the significance of grain crystallographic orientation for DMT, which is central to the Meike, Gratz and Gratier models, has received comparatively little recognition (e.g. Hicks et al., 1986). The observations presented in this contribution that show a significant variation in fracture strength with orientation, suggest that cold work hardening induced microstructures develop preferentially in some grains rather than others. Those grains that develop these microstructures early will be prone to DMT modification due to DESD (i.e. LTP).

6.4. Relationship to faulting processes

The progressive deformation due to grain-contact stress concentration contributes significantly to the faulting cycle. The slow and progressive damage caused by grain indentation is analogous to the aseismic creep component, as follows. Indentation causes the formation of a (LTP) plastic stretch (i.e. δ) zone, which may initially blunt any original flaws and subsequent microcrack development. Eventually, cold work strain hardening, the rate of which is likely to be crystallographically controlled, forces the local stress to exceed the local failure stress and microcracks can begin to advance. Eventually, microcracks coalesce and a significant (seismic) component of crack advance (faulting) is achieved. Simultaneously, the local grain contact deformation can enhance DMT rates, resulting in the potential for fault sealing, such that the fault zone can become (locally) strengthened prior to a repetition of the aseismic–seismic cycle. The progressive intragranular deformation described in this contribution therefore can be viewed as a microcosm of the macroscopic faulting process and explains DMT lithification as a mechanism for stick–slip behaviour of faults (e.g. Angevine et al., 1982) and also porosity reduction (e.g. Angevine and Turcotte, 1983). Thus, the micro-mechanisms of pressure-induced grain scale processes in rocks (e.g. Wong 1990; Zhang et al., 1990; Wheeler 1992) are central to any understanding of faulting.

7. Conclusions

1. SEM FSE and EBSD techniques have been used to study the microstructures that develop due to stress concentrations at grain contacts during faulting of quartzite.

2. The first and most obvious microstructure to develop is dauphiné twins, which occur as classic penetration twins and can induce a preferred orientation of ***r***, from which the maximum compressive stress direction can be inferred.
3. In contrast, dauphiné twinning can diminish any preferred orientation of ***z*** and may therefore reduce whole rock seismic P-wave velocity anisotropy.
4. As dauphiné twinning involves acoustic emissions, care should be taken in attributing all acoustic emissions measured in experimental deformation tests to microfracturing.
5. Dauphiné twinning influences the response of individual quartz grains to deformation depending on the crystal orientation of the grain relative to the imposed stress–strain system and provides an extra degree of freedom to facilitate homogeneous rock deformation by easily forming many of the boundaries that develop in a microstructure.
6. Dauphiné twin microstructures are subsequently overprinted by a zone of coldwork strainhardening comprising a cellular dislocation network that forms a micron-scale subgrain array; such cold-worked strain-hardened microstructures are prone to microfracture to form a (sub)micron-scale cellular array, similar to that observed beneath microhardness indenters.
7. Both subgrain and cellular microstructures assist local DMT processes, particularly in coarse-grain sandstones and quartzites, in a similar manner to that proposed by the models of Meike (1990), Gratz (1991) and Gratier et al. (1999).
8. The progressive deformation due to grain contact stress concentration contributes significantly to the aseismic creep component during the aseismic–seismic faulting cycle; the enhanced DMT possibly aids fault sealing and strengthening, thereby promoting subsequent further fracture.

Acknowledgements

Rob Knipe assisted in the original field work and specimen collection exercise. Discussions with Andy Farmer, Andy Lind, Dave Mainprice, Berndt Neumann, Dave Prior and Pat Trimby regarding EBSD analysis and dauphiné twinning are greatly appreciated. Dave Mainprice is thanked for providing Fig. 10a,b and also for use of his pole figure contouring program (Fig. 10c). CamScan plc and HKL Software plc are thanked for SEM and EBSD assistance, respectively. The comments of Bernd Leiss, Berndt Neumann and an anonymous reviewer helped to improve the original manuscript. This work was supported by UK Natural Environment Research Council (NERC) grants GR3/4461 and GR9/3223 and was presented at the International Conference on Textures and Physical Properties of Rocks, Göttingen, October 1999, via a grant from Sonderforschungsbereich 468.

References

Adams, M., Sines, G., 1978. Crack extensions from flaws in a brittle material subjected to compression. Tectonophysics 49, 97–118.

Anders, M.H., Wiltschko, D.V., 1994. Microfracturing, palaeostress and the growth of faults. Journal of Structural Geology 16, 795–815.

Angevine, C.L., Turcotte, D.L., 1983. Porosity reduction by pressure solution: a theoretical model for quartz arenites. Geological Society of America Bulletin 94, 1129–1134.

Angevine, C.L., Turcotte, D.L., Furnish, M.D., 1982. Pressure solution lithification as a mechanism for stick–slip behaviour of faults. Tectonics 1, 151–160.

Ashby, M.F., Ghandi, C., Taplin, D.M.R., 1979. Fracture mechanics maps and their construction for fcc metals and alloys. Acta Metallurgica 21, 149–163.

Atkinson, B.K., 1987. Fracture Mechanics of Rock. Academic Press, London.

Aydin, A., 1978. Small faults formed as deformation bands in sandstone. Pure and Applied Geophysics 116, 913–930.

Aydin, A., Johnson, A.M., 1993. Analysis of faulting in porous sandstones. Journal of Structural Geology 5, 19–35.

Baker, D.W., Riekels, L.M., 1977. Dauphiné twinning in quartz mylonite. Journal of Geology 85, 15–26.

Baker, D.W., Wenk, H-R., 1972. Preferred orientation in a low-symmetry quartz mylonite. Journal of Geology 80, 81–105.

Barber, D.J., Wenk, H.R., 1991. Dauphine twinning in deformed quartzites—implications of an in-situ TEM study of the alpha–beta phase transformation. Physics and Chemistry of Minerals 17, 492–502.

Berka, L., 1982. On stress distribution in a structure of polycrystals. Journal of Materials Science 17, 1508–1512.

Blenkinsop, T.G., Drury, M.R., 1988. Stress estimates and fault history from quartz microstructures. Journal of Structural Geology 10, 673–684.

Blenkinsop, T.G., Rutter, E.H., 1986. Cataclastic deformation of quartzite in the Moine Thrust Zone. Journal of Structural Geology 8, 669–682.

Bloss, F.D., 1957. Anisotropy of fracture in quartz. American Journal of Science 255, 214–225.

Bowler, S., 1989. Shape fabric formation by cataclasis in a quartzite from the Moine Thrust Zone, Northwest Scotland. Geology 17, 353–356.

Butler, R.W.H., 1984. Structural evolution of the Moine Thrust Belt between Loch More and Glendhu, Sutherland, Scotland. Journal of Geology 20, 161–179.

Butler, R.W.H., Coward, M.P., 1984. Geological constraints, structural evolution and deep geology of the Northwest Scottish Caledonides. Tectonics 3, 347–365.

Christie, J.M., 1963. The Moine Thrust Zone in the Assynt region, Northwest Scotland. University of California Publications in Geological Sciences 40, 345–440.

Coward, M.P., 1983. The thrust and shear zones of the Moine Thrust Zone and NW Scottish Caledonides. Journal of the Geological Society of London 140, 795–811.

Coward, M.P., 1984. The strain and textural history of thin-skinned tectonic zones: examples from the Assynt region of the Moine Thrust Zone, NW Scotland. Journal of Structural Geology 6, 89–100.

Coward, M.P., 1985. The thrust zones of southern Assynt, Moine Thrust Zone. Geological Magazine 122, 595–607.

De Bresser, J.H.P., Spiers, C.J., 1997. Strength characteristics of the r, f and c slip systems in calcite. Tectonophysics 272, 1–23.

den Brok, S.W.J., 1998. Effect of microcracking on pressure solution strain rate: the Graz grain-boundary model. Geology 26, 915–918.

Dingley, D.J. 1999. Orientation relationships between crystals in non-cubic systems, Gottingen Arbeiten Geologie und Palaontologie. Sb4, 35–36.

Dingley, D.J., Randle, V., 1992. Microtexture determination by electron back-scatter diffraction. Journal of Material Science 27, 4545–4566.

Drury, M.R., 1993. Deformation lamellae in metals and minerals. In: Boland, J.N., FitzGerald, J.D. (Eds.), Defects and Processes in the Solid State: Geoscience Applications—The McLaren Volume, Developments in Petrology, 14. Elsevier, Oxford, pp. 195–212.

Elliott, D., Johnson, M.R.W., 1980. Structural evolution in the northern part of the Moine Thrust Zone. Transactions of the Royal Society of Edinburgh 71, 69–96.

Ewalds, H.L., Wanhill, R.J.H. 1989. Fracture Mechanics. Edward Arnold, London, 304 pp.

Farmer, A.B. 1992. A microstructural investigation of natural deformation in quartz aggregates. Unpublished Ph.D. thesis, University of Leeds.

Ferguson, C.C., Lloyd, G.E., Knipe, R.J., 1987. Fracture mechanics and deformation processes in natural quartz: a combined Vickers indentation, SEM and TEM study. Canadian Journal Earth Sciences 24, 544–555.

Field, D.P., 1997. Recent advances in the application of orientation imaging. Ultramicroscopy 67, 1–9.

Fliervoet, T.F., White, S.H., 1995. Quartz deformation in a very fine grained quartzo-feldspathic mylonite: a lack of evidence for dominant grain boundary sliding deformation. Journal of Structural Geology 17, 1095–1109.

Fliervoet, T.F., Drury, M.R., Chopra, P.N., 1999. Crystallographic preferred orientations and misorientations in some olivine rocks deformed by diffusion or dislocation creep. Tectonophysics 303, 1–27.

Freeman, B., Ferguson, C.C., 1986. Deformation mechanism maps and mechanics of rocks with distributed grain sizes. Journal of Geophysical Research 91, 3849–3860.

Frondel, C., 1962. Dana's System of Mineralogy: III Silica Minerals. John Wiley and Sons, New York, p. 334.

Gallagher, J.J., Friedman, M., Handin, J., Sowers, G.M., 1974. Experimental studies relating to microfracture in sandstone. Tectonophysics 21, 203–247.

Ghandi, C., Ashby, M.F., 1979. Fracture-mechanism maps for materials which cleave: fcc, bcc and hcp metals and ceramics. Acta Metallurgica 27, 1565–1602.

Glover, P.W.I., Baud, P., Darot, M., Meredith, P.G., Boon, S.A., Leravalec, M., Zoussi, S., Reuschle, T., 1995. Alpha/beta phase-transition in quartz monitored using acoustic emissions. Geophysical Journal International 120, 775-782.

Goldstein, J.I., Newbury, D.E., Echlin, P., Joy, D.C., Romig Jr, A.D., Lyman, C.E., Fiori, C., Lifshin, E., 1992. Scanning Electron Microscopy and X-ray Microanalysis, 2nd edition. Plenum Press, New York, p. 820.

Gratier, J.P., Renard, F., Labaume, P., 1999. How pressure solution creep and fracturing processes interact in the upper crust to make it behave in both a brittle and viscous manner. Journal of Structural Geology 21, 1189–1198.

Gratz, A.J., 1991. Solution-transfer compaction of quartzites: progress towards a rate law. Geology 19, 901–904.

Green, H.W., Griggs, D.T., Christie, J.M., 1970. Syntectonic and annealing recrystallisation of fine-grained quartz aggregates. In: Paulitsch, P. (Ed.). Experimental and Natural Rock Deformation. Springer-Verlag, New York, pp. 272–335.

Griggs, D.T., Turner, F.J., Heard, H.C., 1960. Deformation of rocks at 500 to 800°C. Geological Society of America Memoir 79, 39–105.

Groshong, R.H., 1988. Low-temperature deformation mechanisms and their interpretation. Geological Society of America Bulletin 100, 1329–1360.

Groshong, R.H., Teufel, L.W., Gasteiger, C., 1984. Precision and accuracy of the calcite strain-gauge technique. Geological Society of America Bulletin 95, 357–363.

Gurtovoi, V.L., Eremenko, V.G., 1991. Visualisation of dauphine twin boundaries in a quartz filter by electron acoustic microscopy. Soviet Physics Acoustics—USSR 37, 597–600.

Hicks, B.D., Applin, K.R., Houseknecht, D.W., 1986. Crystallographic influences on intergranular pressure solution in a quartzose sandstone. Journal of Sedimentary Petrology 56, 784–787.

Hippler, S.J., Knipe, R.J., 1990. The evolution of cataclastic rocks from a pre-existing mylonite. In: Knipe, R.J., Rutter, E.H. (Eds.), Deformation Mechanisms, Rheology and Tectonics. Special Publication 54. Geological Society, London, pp. 71–80.

Hirth, G., Tullis, J., 1992. Dislocation creep regimes in quartz aggregates. Journal of Structural Geology 14, 145–159.

Hirth, G., Tullis, J., 1994. The brittle-plastic transition in experimentally deformed quartz aggregates. Journal of Geophysical Research 99, 11731–11747.

Houseknecht, D.W., 1984. Influence of grain size and temperature on intergranular pressure solution, quartz cementation and porosity in a quartzose sandstone. Journal of Sedimentary Petrology 54, 348–361.

Houseknecht, D.W., 1988. Intergranular pressure solution in four quartzose sandstones. Journal of Sedimentary Petrology 58, 228–246.

Johnson, M.R.W., Kelley, S.P., Oliver, G.J.H., Winter, D.A.., 1985. Thermal effects and timing of thrusting in the Moine Thrust Zone. Journal Geological Society of London 142, 863–874.

Jones, G., Fisher, Q.J., Knipe, R.J., 1998. Faulting, Fault Sealing and Fluid Flow in Hydrocarbon Reservoirs, Special Publication 147, Geological Society, London, pp. 117–134.

Kirby, S.H., 1984. Introduction and special digest to the special issue on chemical effects of water on the deformation and strength of rocks. Journal of Geophysical Research 89, 3991–3995.

Knipe, R.J., 1989. Deformation mechanisms—recognition from natural tectonites. Journal of Structural Geology 11, 127–146.

Knipe, R.J., 1990. Microstructural analysis and tectonic evolution in thrust systems: examples from the Assynt region of the Moine Thrust Zone, NW Scotland. In: Barber, D.J., Meredith, P.G. (Eds.), Deformation Processes in Minerals, Ceramics and Rocks. Mineralogical Society Special Publication 1. Unwin Hyman, London.

Knipe, R.J., 1992a. Faulting processes and fault seal. In: Larsen, R.M., Brekke, H., Larsen, B.T., Talleraas, E. (Eds.), Structural and Tectonic Modelling and its Applications to Petroleum Geology. Elsevier, Amsterdam, pp. 325–345.

Knipe, R.J., 1992b. Micromechanisms of deformation and fluid flow behaviour during faulting. Mechanical Involvement of Fluids in Faults, USGS Proceedings of Workshop LXIII. Open File Report, pp. 94–228.

Knipe, R.J., Lloyd, G.E., 1994. Microstructural analysis of faulting in quartzite, Assynt, NW Scotland: implications for fault zone evolution. Pure and Applied Geophysics 143, 229–254.

Knipe, R.J., Rutter, E.H., 1990. Deformation Mechanisms, Rheology and Tectonics. Special Publication 54. Geological Society, London, pp. 71–80.

Knott, J.F., 1979. Fundamentals of Fracture Mechanics. Butterworths, London.

Kranz, R.L., 1983. Microcracks in rocks: a review. Tectonophysics 101, 449–480.

Lapierre, J., Mainprice, D, Ben Ismail, W., 1996. A method for calculating rock physical properties from published pole figures. In: De Paor, D.G. (Ed.), Structural Geology and Personal Computers. Pergamon, Oxford, pp. 167–178.

Larsen, R.M., Brekke, H., Larsen, B.T., Talleraas, E., 1992. Structural and Tectonic Modelling and its Applications to Petroleum Geology. Elsevier, Amsterdam, pp. 325–345.

Lind, A. 1996. Microstructural stability and the kinetics of textural evolution. Unpublished Ph.D. thesis, University of Leeds.

Linker, M.F., Kirby, S.H., Ord, A., Christie, J.M., 1984. Effects of compression direction on the plasticity and rheology of hydrolytically weakened synthetic quartz crystals at atmospheric pressure. Journal of Geophysical Research 89, 4241.

Lloyd, G.E., 1987. Atomic number and crystallographic contrast images with the SEM: a review of backscattered electron techniques. Mineralogical Magazine 51, 3–19.

Lloyd, G.E., Farmer, A.B., Mainprice, D., 1997. Misorientation analysis

and the formation and orientation of subgrain and grain boundaries. Tectonophysics 279, 55–78.

Lloyd, G.E., Freeman, B., 1991. SEM electron channelling analysis of dynamic recrystallisation in a quartz grain. Journal of Structural Geology 13, 945–953.

Lloyd, G.E., Freeman, B., 1994. Dynamic recrystallisation of quartz and quartzites. Journal of Structural Geology 16, 867–881.

Lloyd, G.E., Knipe, R.J., 1992. Deformation mechanisms accommodating faulting of quartzite under upper crustal conditions. Journal of Structural Geology 14, 127–143.

Lloyd, G.E., Law, R.D., Mainprice, D., Wheeler, J., 1992. Microstructural and crystal fabric evolution during shear zone formation. Journal of Structural Geology 14, 1079–1100.

Lloyd, G.E., Schmidt, N.-H., Mainprice, D., Prior, D.J., 1991. Crystallographic textures. Mineralogical Magazine 55, 331–345.

Mainprice, D., Humbert, M., 1994. Methods of calculating petrophysical properties from lattice preferred orientation data. Survey Geophysics 15, 575–592.

Mainprice, D., Lloyd, G.E., Casey, M., 1993. Individual orientation measurements in quartz polycrystals-advantages and limitations for texture and petrophysical property determinations. Journal of Structural Geology 15, 1169–1187.

Marone, C.J., Blanpied, M.J., 1994. Special Issue: Faulting, Friction and Earthquake Mechanics. Pure and Applied Geophysics 143, 1–511.

Marone, C., Scholz, C.H., 1989. Particle size distribution and microstructures within simulated fault gouge. Journal of Structural Geology 11, 799–814.

McClay, K.R., Coward, M.P., 1981. The Moine Thrust Zone: An Overview. In: McClar, K.R., Price, N.J. (Eds.), Thrust and Nappe Tectonics. Special Publication 9. Geological Society, London, pp. 241–260.

McGrath, A.G., Davison, I., 1995. Damage zone geometry around fault tips. Journal of Structural Geology 17, 1011–1024.

McLaren, A.C., 1986. Some speculations on the nature of high-angle grain boundaries in quartz rocks. In: Hobbs, B.E., Heard, H.C. (Eds.), Mineral and Rock Deformation: Laboratory Studies, The Paterson Volume, Geophysical Monograph Series, 36. American Geophysical Union, Washington, pp. 233–247.

McSkimin, H.J., Andreatch, P., Thurston, R.N., 1965. Elastic moduli of quartz versus hydrostatic pressure at 25°C and −195.8°C. Journal of Applied Physics 36, 1624–1632.

Meike, A., 1990. Dislocation enhanced selective dissolution: an examination of mechanical aspects using deformation mechanism maps. Journal of Structural Geology 12, 785–794.

Menendez, B., Zhu, W., Wong, T., 1996. Micromechanics of brittle faulting and cataclastic flow in Brea sandstone. Journal of Structural Geology 18, 1–16.

Mitra, G., 1984. Ductile deformation zones and mylonites: the mechanical processes involved in the deformation of crystalline basement rocks. American Journal of Science 278, 1057–1084.

Mitra, S., 1988. Effects of deformation mechanisms on reservoir potential in Central Appalachian overthrust belt. American Association of Petroleum Geologists Bulletin 72, 536–554.

Moore, D.E., Lockner, D.A., 1995. The role of microfracturing in shear fracture propagation in granite. Journal of Structural Geology 17, 95–114.

Neumann, B. 1996. Texturbildende Prozesse in rekristallisierten Quarzpolykristallen. Geotektonische Forschungen 87. University of Gottingen, Germany, 154 pp.

Nicolas, A., Poirier, J.P., 1976. Crystalline Plasticity and Solid State Flow in Metamorphic Rocks. John Wiley, London.

Nord, G.L., 1994. Transformation-induced twin boundaries in minerals. Phase Transitions 48, 107–134.

Olesen, N.O., Schmidt, N.H., 1990. The SEM/ECP technique applied on twinned quartz crystals. In: Knipe, R.J., Rutter, E.H. (Eds.), Deformation Mechanisms, Rheology and Tectonics. Special Publication 54. Geological Society, London, pp. 369–374.

Peach, B.N., Horne, J., Gunn, W., Clough, C.T., Hinxman, L.W., 1907. The geological structure of the Northwest Highlands of Scotland, Memoir, Geological Survey of Great Britain.

Prior, D.J., 1999. Problems in determining the orientation of crystal misorientation axes for small angular misorientations, using electron backscatter diffraction in the SEM. Journal of Microscopy 195, 217–225.

Prior, D.J., Boyle, A.P., Brenker, F., Cheadle, M.C., Day, A., Lopez, G., Potts, G.J., Reddy, S., Spiess, R., Timms, N., Trimby, P., Wheeler, J., Zetterstrom, L., 1999. The application of electron backscatter diffraction and orientation contrast imaging in the SEM to textural problems in rocks. American Mineralogist 84, 1741–1759.

Putnis, A., 1992. Introduction to Mineral Sciences. Cambridge University Press, Cambridge, p. 457.

Rutter, E.H., 1983. Pressure solution in nature, theory and experiment. Journal of the Geological Society of London 140, 725–740.

Rutter, E.H., 1995. Experimental study of the influence of stress, temperature and strain on the dynamic recrystallisation of Carrara marble. Journal of Geophysical Research 100, 24651–24663.

Rutter, E.H., Maddock, R.H., Halls, S.H., White, S.H., 1986. Comparative microstructures of natural and experimentally produced clay-bearing fault gouges. Pure and Applied Geophysics 124, 3–30.

Schmidt, N.-H., Olesen, N.O., 1989. Computer-aided determination of crystal lattice orientation from electron channelling patterns in the SEM. Canadian Mineralogist 27, 15–22.

Schmidt-Mumm, A., 1991. Low frequency acoustic emission from quartz upon heating from 90 to 610 degrees C. Physics and Chemistry of Minerals 17, 553–565.

Schneibel, J.H., Coble, R.L., Cannon, R.M., 1981. The role of grain size distribution in diffusional creep. Acta Metallurgica 29, 1285–1290.

Scholtz, C.H., 1989. Mechanics of faulting. Annual Review of Earth and Planetary Sciences 17, 309–334.

Sibson, R.H., 1986. Earthquakes and rock deformation in crustal fault zones. Annual Review of Earth and Planetary Sciences 14, 149–175.

Snoke, A.W., Tullis, J., Todd, V.R., 1998. Fault-related Rocks: A Photographic Atlas, Princeton University Press, Princeton, NJ, p. 617.

Swett, K. 1969. Interpretation of the depositional and diagenetic history of the Cambro-Ordovician succession of Northwest Scotland. In: Kay, M. (Ed.), North Atlantic—Geology and Continental Drift. Memoir, American Association of Petroleum Geologists 12, 630–646.

Thomas, L.A., Wooster, W.A., 1951. Piezocrescence—the growth of Dauphiné twinning in quartz under stress. Proceedings of the Royal Society of London Series A208, 43–62.

Trimby, P.W., Prior, D.J., 1999. Microstructural imaging techniques: a comparison between light and scanning electron microscopy. Tectonophysics 303, 71–81.

Trimby, P.W., Prior, D.J., Wheeler, J., 1998. Grain boundary hierarchy development in a quartz mylonite. Journal of Structural Geology 20, 917–935.

Tullis, J.A., 1970. Quartz preferred orientation in rocks produced by Dauphiné twinning. Science 168, 1342–1344.

Tullis, J.A., 1971. Preferred orientations of experimentally deformed quartzites. Ph.D. thesis, University of California, Los Angeles, p. 344.

Tullis, T.E., 1980. The use of mechanical twinning in minerals as a measure of shear stress magnitudes. Journal of Geophysical Research 85, 6263–6268.

Tullis, T.E., 1986. Special issue: Friction and Faulting. Pure and Applied Geophysics 124, 375–608.

Tullis, J.A., Tullis, T., 1972. Preferred orientation of quartz produced by mechanical twinning: thermodynamics and axial experiments. 'Flow and Fracture of Rocks—the Griggs Volume'. American Geophysical Union 16, 67–82.

Turner, F.J., 1962. 'Compression' and 'tension' axes determined from {0112} twinning in calcite. Journal of Geophysical Research 67, 1660.

Underhill, J.R., Woodcock, N.H., 1987. Faulting mechanisms in high porosity sandstones, New Red Sandstones, Arran, Scotland. In: Jones, M.E., Preston, R.M.F. (Eds.), Deformation of Sediments and Sedimentary Rocks. Special Publication 29. Geological Society, London, pp. 91–105.

Vermilye, J.M., Scholz, C.H., 1998. The process zone: a microstructural view of fault growth. Journal of Geophysical Research 103, 12223–12237.

Vermilye, J.M., Scholz, C.H., 1999. Fault propagation and segmentation: insight from the microstructural examination of a small fault. Journal of Structural Geology 21, 1623–1636.

Wang, C.H., 1986. Special issue: Internal Structure of Fault Zones. Pure and Applied Geophysics 124, 373pp.

Weathers, M.S., Bird, J.M., Cooper, R.F., Kohlstedt, D.C., 1979. Differential stress determination from deformation induced microfractures in the Moine Thrust Zone. Journal of Geophysical Research 84, 7495–7509.

Wheeler, J., 1987. The significance of grain scale stresses in the kinetics of metamorphism. Contributions to Mineralogy and Petrology 17, 397–404.

Wheeler, J., 1992. The importance of pressure solution and Coble creep in the deformation of polymineralic rocks. Journal of Geophysical Research 97, 4579–4586.

Wilkinson, A.J., Hirsch, P.B., 1997. Electron diffraction based techniques in scanning electron microscopy of bulk materials. Micron 28, 279–308.

Wintsch, R.P., Dunning, J., 1985. The effect of dislocation density on aqueous solubility of quartz and some geological implications. Journal of Geophysical Research 90, 49–57.

Wong, T.-F., 1990. Mechanical compaction and the brittle–ductile transition in porous sandstones. In: Knipe, R.J., Rutter, E.H. (Eds.), Deformation Mechanisms, Rheology and Tectonics. Special Publication 54. Geological Society, London, pp. 111–122.

Wong, T.-F., David, C., Zhu, W., 1997. The transition from brittle faulting to cataclastic flow in porous sandstones: mechanical deformation. Journal of Geophysical Research 102, 3009–3025.

Zhang, S., Wong, T.-F., Davis, D.M., 1990. Micromechanisms of pressure-induced grain crushing in porous rocks. Journal of Geophysical Research 95, 341–352.